

**R-matrix analysis of Cl neutron cross sections up to 1.2 MeV**

R. O. Sayer,\* K. H. Guber, L. C. Leal, and N. M. Larson

*Nuclear Science and Technology Division, Oak Ridge National Laboratory, P.O. Box 2008, Oak Ridge, Tennessee 37831, USA*

T. Rauscher

*Institut für Physik, Universität Basel, Klingelbergstr. 82, CH-4056 Basel, Switzerland*

(Received 28 September 2005; published 3 April 2006)

We have analyzed and evaluated  $^{35}\text{Cl}$ ,  $^{37}\text{Cl}$ , and  $^{\text{nat}}\text{Cl}$  neutron cross section data in the resolved resonance region with the multilevel Reich-Moore  $R$ -matrix formalism. Energies and widths were determined for 388 resonances in the range 0.2 to 1200 keV. New  $J$  assignments were made for 33 resonances, and parities were assigned for 15 of these resonances. Neutron strength functions were calculated for both  $s$  and  $p$  waves; our results include the first reported  $p$ -wave values for Cl. Resonance analyses were carried out with the computer code SAMMY, which utilizes Bayes' method, a generalized least-squares technique. Because SAMMY now has the ability to calculate charged-particle penetrabilities, it was possible to include a proton exit channel in the analysis and to deduce proton widths for several resonances. Our resonance parameter representation describes the data much better than previous evaluations, and it should lead to improved criticality safety calculations for systems where Cl is present.

DOI: [10.1103/PhysRevC.73.044603](https://doi.org/10.1103/PhysRevC.73.044603)

PACS number(s): 27.30.+t, 21.10.Pc, 24.30.Gd, 28.20.-v

**I. INTRODUCTION**

Recently Guber *et al.* [1] reported new high-resolution capture and transmission measurements of  $^{\text{nat}}\text{Cl}$  up to 600 keV at the Oak Ridge Electron Linear Accelerator (ORELA). They performed a resonance parameter analysis and computed keV Maxwellian averaged cross sections and reaction rates for  $^{35}\text{Cl}$  and  $^{37}\text{Cl}$ . In the present work, we have extended the resonance parameter analysis up to 1.2 MeV, taking into account all known older measurements as well as the new ORELA data. We have made new  $J^\pi$  assignments for 15 resonances, made new  $J$  assignments for 18 additional resonances, deduced energies and widths for 388  $s$ - and  $p$ -wave resonances, and computed neutron strength functions and average level spacings. Since the multilevel Reich-Moore  $R$ -matrix formalism in the code SAMMY [2] has the capability to calculate charged-particle penetrabilities, we were able to fit the  $^{35}\text{Cl}(n,p)$  data and to extract proton widths for several resonances. A brief report of our Cl cross section analysis has been published previously [3].

An important motivation for the work described herein arose from the impact of Cl neutron cross sections on criticality safety computations; for example, polyvinyl chloride pipe is 57% Cl by weight. Several deficiencies in the existing ENDF/B-VI data evaluation [4] for Cl have been noted [1]; the present work addresses these deficiencies and provides a significantly more accurate representation of the data than previous evaluations. In the following sections we discuss the cross section data, resonance analyses, average quantities, and conclusions.

**II. RESONANCE ANALYSIS AND RESULTS**

Resonance parameters were determined by a consistent analysis in which corrections for Doppler broadening,

resolution broadening, multiple scattering, and other experimental effects were incorporated. Data sets were analyzed sequentially so that each fit was connected to the previous fit by the SAMMY parameter covariance matrix, thereby yielding energies and widths for 82  $s$ -wave and 306  $p$ -wave resonances in the neutron energy range 0.2–1200 keV. Of these 388  $s$ - and  $p$ -wave resonances, 246 were assigned to  $^{35}\text{Cl}$  and 142 to  $^{37}\text{Cl}$ . To fit off-resonant cross sections, it is necessary to consider the effect of resonances and bound states external to the energy region of interest. In SAMMY, this can be done either with an external  $R$  function or with *dummy* resonances; we chose the latter option. Three negative-energy resonances were included to account for bound levels, and several high-energy resonances were included to account for the effect of resonances above 1200 keV.

Fits were obtained for recent ORELA transmission and capture data [1] as well as for several older cross section data sets. Standard nuclear databases and the open literature were searched for capture, total, and reaction cross section data. Selected information about the data sets used in our analysis is listed in Table I.

Definite spin values were assigned for 39 resonances in  $^{35}\text{Cl}$  and 7 resonances in  $^{37}\text{Cl}$  on the basis of detailed shape and area analysis of capture and transmission data. Definite parity assignments were made for 45 resonances.

In order to give a proper treatment for charged particles in an exit channel, an algorithm to calculate charged-particle penetrabilities (CPP) and shifts was incorporated in the SAMMY code. The methodology [14] for CPP computation is given in the appendix.

The nuclear radii used for penetrabilities and shifts were computed according to  $R = 1.23A^{1/3} + 0.8$  fm, where  $A$  is the nuclide mass. These values were 4.8222 and 4.8974 fm for  $^{35}\text{Cl}$  and  $^{37}\text{Cl}$ , respectively. Off-resonant fits are affected not only by the *dummy* resonances, but also by the radii used to compute hard-sphere phase shifts. We obtained better fits by varying the “hard-sphere” radii  $R_\phi$  with different values

\*Corresponding author: [sayerro@ornl.gov](mailto:sayerro@ornl.gov)

TABLE I. Data sets for  $^{35,37}\text{natCl}$  evaluation.

Data type	Lead author	Facility	Flight path (m)	Energy analysis range (keV)
Trans.	Guber [1]	ORELA	79.82	0.02–1250
Trans.	Good [5]	ORELA	78.20	0.38–0.42
Total	Singh [6]	Columbia cyclotron	202.05	0.02–400
Total	Brugger [7]	MTR fast chopper	45	0.03–15
Total	Cierjacks [8]	KFK cyclotron	57.54	500–1250
Total	Kiehn [9]	Rockefeller generator		133–1084
Total	Newson [10]	Duke Van de Graaff		7–194
Capt.	Guber [1]	ORELA	40	0.1–500
Capt.	Kashukeev [11]			0.022–1
( $n,p$ )	Koehler [12]	LANSCE		0.000025–35
( $n,p$ )	Druyts [13]	GELINA	8, 30	0.3–110

allowed for  $s$  and  $p$  waves. It should be noted that the  $R_\phi$  values and some of the *dummy* resonance parameters tend to be highly correlated. Thus, it is quite possible that an equally good fit to the data could be found with another set of *dummy* resonances and somewhat different  $R_\phi$  values. Final values for  $^{35}\text{Cl}$  were  $R_\phi(l=0,1) = 3.6680, 4.8888$  fm; final values for  $^{37}\text{Cl}$  were  $R_\phi(l=0,1) = 3.3651, 3.9565$  fm. Our Cl  $s$ -wave  $R_\phi$  values are consistent with experimental values (see Fig. 1 of Ref. [15]) of potential scattering radii in this mass region.

For neutron energy  $E_n < 1$  keV, Fig. 1 shows a global view of the final SAMMY fits to the total cross section values of Refs. [1,7], the  $^{35}\text{Cl}(n,p)$  cross section values of Ref. [12], and the capture data of Ref. [11]. Also shown are the thermal values from ENDF/B-VI.

Below the first resonance at 398 eV, the magnitude and shape of the cross section is determined by the  $^{35}\text{Cl}(n,p)$  data of Ref. [12], the total cross section data of Ref. [7], the transmission data of Ref. [1], and the well-known thermal values [15]. These data were analyzed sequentially to obtain parameters for the bound state at  $-180$  eV.

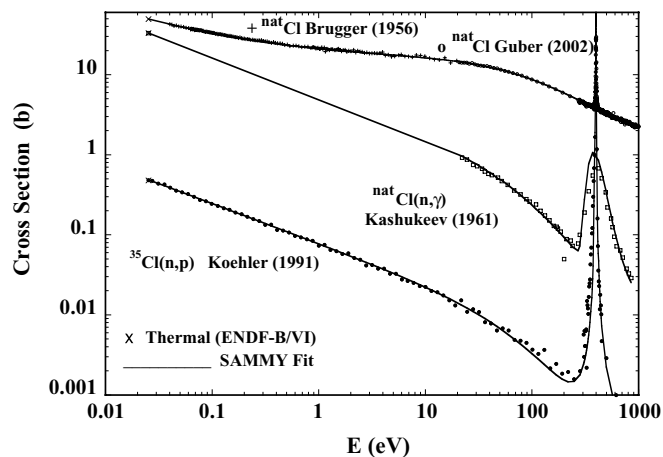


FIG. 1. Comparison of SAMMY fits (solid lines) to the  $^{nat}\text{Cl}$  total cross section data of Brugger *et al.* [7] (+ symbols) and Guber *et al.* [1] (open circles); the  $^{nat}\text{Cl}$  capture data of Kashukeev *et al.* [11] (open squares); and the  $^{35}\text{Cl}(n,p)$  data of Koehler [12] (solid circles). The  $\times$  symbols denote the ENDF/B-VI thermal values.

### A. Total cross section analysis

Guber *et al.* [1] measured the transmission of a natural  $\text{CCl}_4$  sample (thickness of Cl, 0.2075 atoms/b) over the range  $0.020 < E_n < 1500$  keV using the 80-m flight path at ORELA. These data exhibit much higher energy resolution and lower background than the older data sets included in our evaluation. This high resolution is shown in Fig. 2, where the SAMMY fits are compared with the transmission data for  $0 < E_n < 500$  keV. Since this sample was too thick to give an accurate neutron width for the 398-eV resonance, we also fit the transmission data of Good *et al.* [5], who used a sample of thickness 0.00812 atoms/b.

Cierjacks *et al.* [8] measured total cross sections for the range  $500 < E_n < 1250$  keV using a 57-m flight path with a burst width of 1 ns from the Kernforschungszentrum Karlsruhe (KFK) Isochronous Cyclotron. A natural  $\text{CCl}_4$  sample of thickness 0.262 atoms/b and chemical purity 99% was utilized. The Cierjacks data were normalized to the data of Guber *et al.* [1] by integrating over the energy range 500–1200 keV. The normalization factor was 1.054. A neutron energy transformation was applied to the Cierjacks data to make the peak energies consistent with the corresponding ORELA values. Examples of SAMMY fits to the Cierjacks and Guber data are presented in Fig. 3. The Cierjacks data and fit were shifted upward for display purposes.

Brugger *et al.* [7] utilized the Materials Testing Reactor (MTR) fast chopper with a flight path of 45 m to measure transmission values over the range 16 eV to 15 keV. They also used the MTR crystal spectrometer for measurements over the range 0.03 to 70 eV. A  $\text{CCl}_4$  sample of thickness  $2.115 \text{ g/cm}^2$  was used with the MTR crystal spectrometer;  $\text{CCl}_4$  and  $\text{NaCl}$  samples were used with the MTR fast chopper. Figure 4 shows a comparison of  $\sigma_{\text{total}}$  values computed from our resonance parameters with the data of Brugger *et al.* [7] and Guber *et al.* [1] for  $0.01 \text{ eV} < E_n < 1 \text{ keV}$ . The higher precision ORELA data, which begin at 20 eV, determine the fit above 20 eV. Brugger *et al.* [7] state that their measurement precision is very good up to 10 eV, and our calculated values agree with the Brugger data (average of 6 points) to better than 2% for  $0.04 < E_n < 3 \text{ eV}$ .

Near 0.03 eV, the cross section computed from our resonance parameter representation and the fit by Brugger *et al.* are

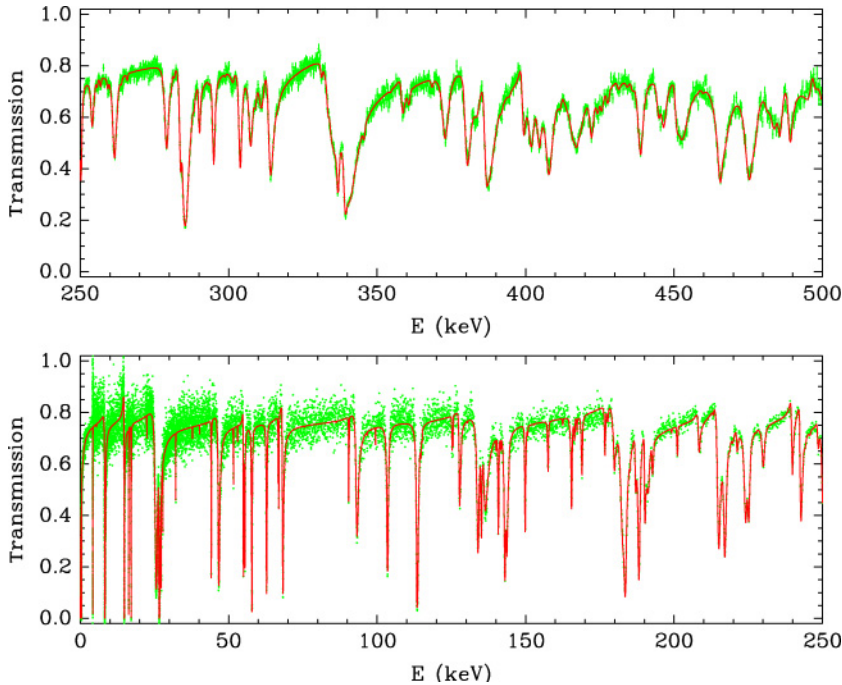


FIG. 2. (Color online) Comparison of SAMMY fits (solid lines) to the  $^{nat}\text{Cl}$  transmission data of Guber *et al.* [1] for  $0 < E_n < 500$  keV.

about 3% higher than the Brugger data. We note that Brugger *et al.* did not correct their data for second-order effects in the monochromating crystal; this correction would increase the

experimental values at the lowest energies and produce better agreement with the predicted values. The SAMMY sequential analysis produced a normalization of 0.992 for the Brugger data.

Singh *et al.* [6] used the 200-m flight path at the Columbia synchrotron to measure transmissions and determine total cross sections for  $^{nat}\text{Cl}$  for samples of thickness 0.198, 0.307, and 0.00764 atoms/b over the energy range 0.02–400 keV. The authors state that their background determination is rather uncertain above 100 keV, and that below 100 eV they adjusted their background values to fit the data of Brugger *et al.* near 20 and 100 eV. For several energy ranges (0.03–1, 115–180, 205–400 keV), the Singh data differ from the more recent high-resolution ORELA data [1] by 10–20%. Consequently, we deemphasized the regions between resonances by

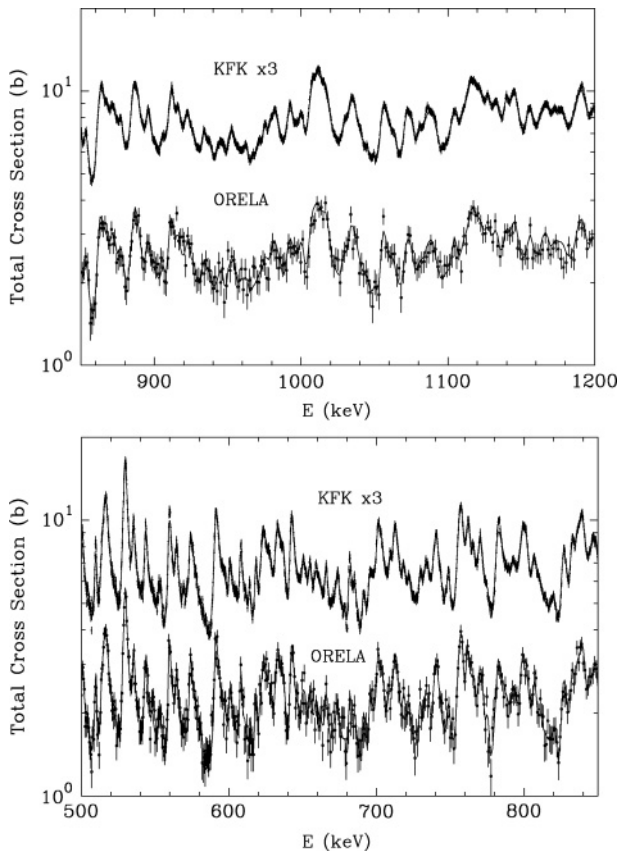


FIG. 3. Comparison of SAMMY fits (solid lines) to the  $^{nat}\text{Cl}$  total cross section data of Cierjacks *et al.* [8] (KFK) and Guber *et al.* [1] (ORELA) for  $500 < E_n < 1200$  keV.

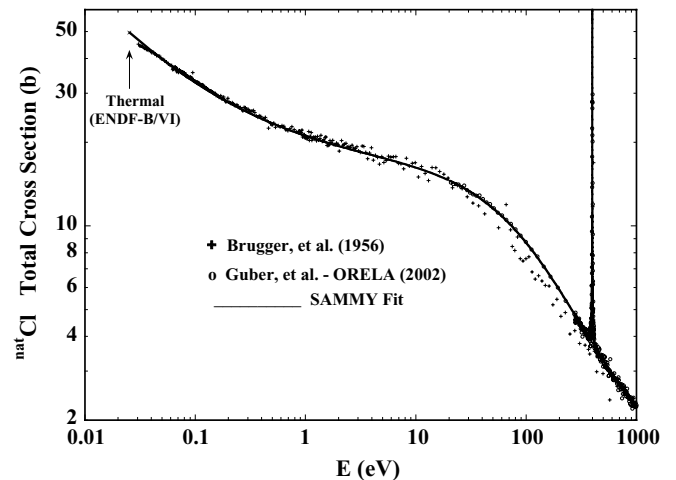


FIG. 4. Comparison of SAMMY fits (solid line) to the  $^{nat}\text{Cl}$  total cross section data of Brugger *et al.* [7] (+ symbols) and Guber *et al.* [1] (open circles). The ENDF/B-VI thermal value is shown as an x.

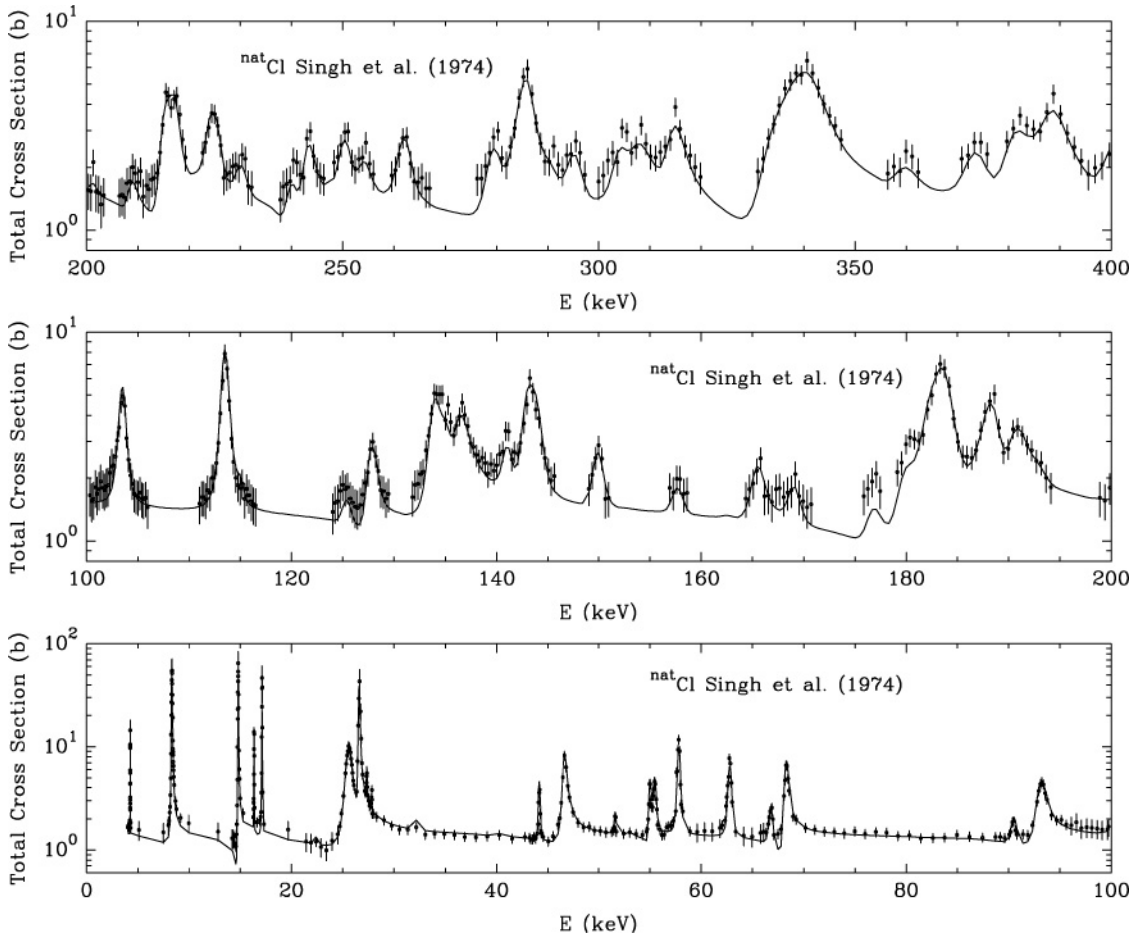


FIG. 5. Comparison of SAMMY fits (solid line) to the  $^{nat}\text{Cl}$  total cross section data of Singh *et al.* [6] for 4–400 keV.

averaging the Singh data and assigning large uncertainties. Doppler and resolution broadening were taken into account in the fits. Since uncertainties were not available for the Singh data, values of 10% were assigned near resonances, and the normalization was varied in the analysis. Results of the SAMMY fits are shown in Fig. 5.

### B. $(n, p)$ cross section analysis

The  $^{35}\text{Cl}(n, p)^{35}\text{S}$  data of Koehler [12] and Druyts *et al.* [13] were analyzed with the SAMMY code, which was modified to compute charged-particle penetrabilities. The  $Q$  value for the  $^{35}\text{Cl}(n, p)^{35}\text{S}$  reaction is  $+0.61522$  MeV.

A wide range of  $^{35}\text{Cl}(n, p)$  thermal cross section values has been reported [15] from both activation and proton-emission experiments. In 1991, Koehler chose to normalize his data to the most accurate value then available,  $489 \pm 14$  mb, measured by Sims and Juhnke [16] and recommended by Mughabghab *et al.* [15]. Sims and Juhnke made activation measurements relative to a  $^{59}\text{Co}$  thermal cross section of 37.5 b. With the more recent value [15] for  $^{59}\text{Co}$ , 37.18 b, and a  $^{35}\text{Cl}$  abundance of 0.7577, we obtain  $483 \pm 14$  mb for the  $^{35}\text{Cl}(n, p)$  thermal cross section.

More recently (1994), Druyts *et al.* [13] observed protons emitted from AgCl samples exposed to thermal neutrons from the ILL (Grenoble) High Flux Reactor. They reported a cross

section of  $440 \pm 10$  mb, which is significantly lower than the best activation value. However, an earlier proton-emission measurement by Schroder *et al.* [17] gave a thermal cross section of  $466 \pm 40$  mb, a value based on  $\sigma_{\text{thermal}} = 4.30 \pm 0.34$  b for  $^{40}\text{K}(n, p_0)$ . Furthermore, Gledenov *et al.* [18] recently reported a much larger value,  $575 \pm 13$  mb, for the  $^{35}\text{Cl}(n, p)$  thermal cross section.

In the  $^{35}\text{Cl}(n, p)$  analysis, we tried data normalizations that corresponded to varying the thermal  $(n, p)$  cross section from 440 to 483 mb. For resonances at 0.398 and 4.251 keV,  $\Gamma_p$  is a significant fraction of the total width; hence  $\sigma_{\text{total}}$  and  $\sigma_\gamma$  are sensitive to  $\Gamma_p$ . In addition,  $\Gamma_p$  depends on the resonance strengths  $g\Gamma_n\Gamma_p/\Gamma$  deduced by Koehler and Druyts *et al.* from area analysis of their peaks. Thus,  $\Gamma_p$  and normalization values must give resonance strengths consistent with experimental peak areas as well as satisfactory fits to the transmission, capture, and  $^{35}\text{Cl}(n, p)$  data. We could not find acceptable fits to all the data with a normalization significantly lower than  $\sigma_{\text{thermal}} = 483$  mb.

SAMMY fits are compared with the data of Koehler in Fig. 1 and Druyts *et al.* in Fig. 6. Between resonance peaks, the Druyts data were very uncertain; therefore, we fit only the peak regions.

Proton, neutron, and capture widths used in our evaluation are given in Table II for resonances seen in the  $^{35}\text{Cl}(n, p)$  data. Resonance strengths  $\omega = g\Gamma_n\Gamma_p/\Gamma$  from our evaluation are

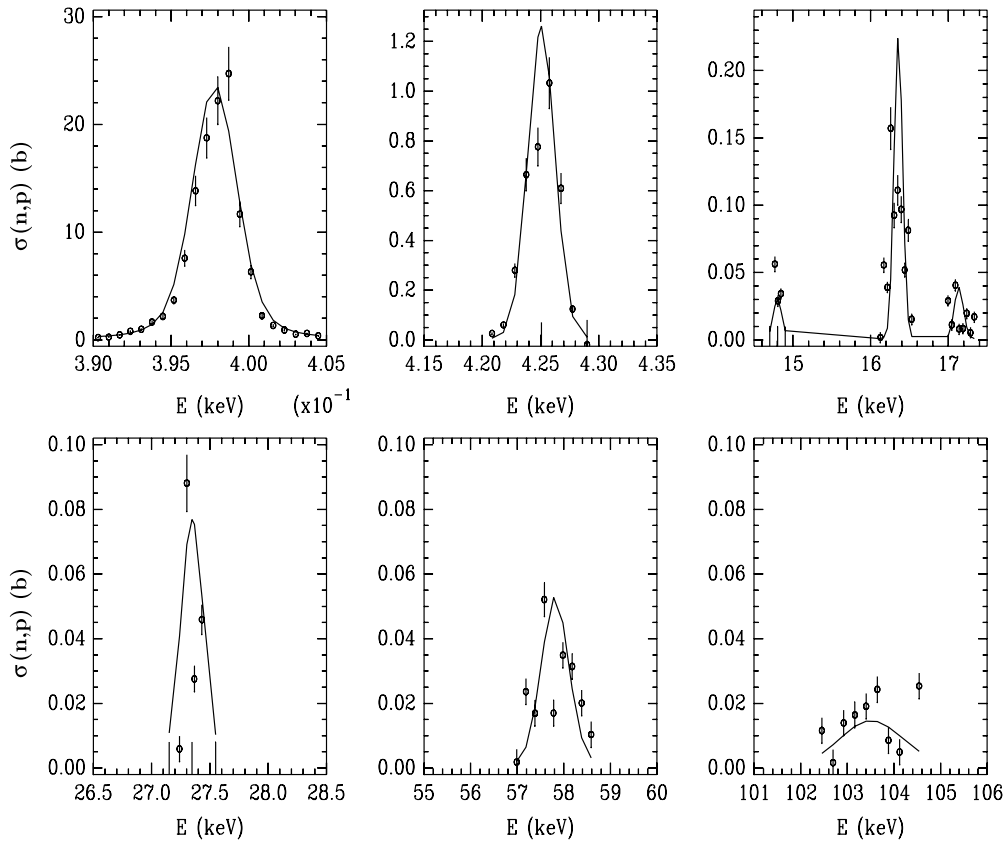


FIG. 6. Comparison of SAMMY fits (solid line) to the  $^{35}\text{Cl}(n,p)$  cross section data of Druyts *et al.* [13] for selected resonances.

compared with corresponding values of Koehler, Druyts *et al.*, and Gledenov *et al.* [19]. For  $E \geq 14.8$  keV, the  $\Gamma_p$  values were computed from the  $\omega$  values of Druyts *et al.* All values in Table II are normalized to  $\sigma_{\text{thermal}} = 483$  mb.

### C. Capture cross section analysis

Guber *et al.* [1] measured the neutron capture of chlorine up to 500 keV using a natural LiCl sample of thickness 0.09812 atoms/b and the ORELA capture system, which

had been reengineered [20] to minimize the amount of structural material surrounding the sample and detectors. To calculate accurate correction factors for experimental effects of the neutron capture data, reliable neutron widths were needed since the sample was fairly thick. Initial  $\Gamma_n$  values were obtained by fitting the transmission data; using these newly determined  $\Gamma_n$  values, corrections for self-shielding and multiple scattering were calculated with SAMMY and used to determine capture widths. Several iterations of fitting the transmission and capture data were

TABLE II. Proton widths and resonance strengths  $\omega = g\Gamma_n\Gamma_p/\Gamma$  for  $^{35}\text{Cl}(n,p)$  from the present evaluation compared with the data of Druyts *et al.* [13], Koehler [12], and Gledenov *et al.* [19]. All data are normalized to a thermal cross section of 483 mb.

$E$ (eV)	$J$	$\Gamma_\gamma$ (meV)	$\Gamma_n$ (meV)	$\Gamma_p$ (meV)	$\omega$ (meV)	$\omega$ [Druyts] (meV)	$\omega$ [Koehler] (meV)	$\omega$ [Gledenov] (meV)
-180.65	2	530	13277	5.99				
397.8	2	665	50.5	$322 \pm 21$	$9.8 \pm 0.9$	$9 \pm 1$	10	$10.8 \pm 1.6$
4250.8	1	472	628	$230 \pm 22$	$40.8 \pm 5.1$	$42 \pm 3$	35	$40.0 \pm 8.0$
14801.9	2	346	32600	28 <sup>a</sup>		$18 \pm 5$		
16356.1	(3)	386	5982	164 <sup>a</sup>		$131 \pm 16$	64	
17133.9	3	802	14096	32 <sup>a</sup>		$26 \pm 9$		
27346.4	(2)	458	6028	147 <sup>a</sup>		$82 \pm 22$	69	
51608.0	(3)	45	2417	96 <sup>a</sup>		$79 \pm 40$		
57811.6	(2)	538	107389	998 <sup>a</sup>		$615 \pm 121$	860	
90420.2	(2)	716	21788	274 <sup>a</sup>		$165 \pm 66$		
103515.4	1	388	381952	1973 <sup>a</sup>		$735 \pm 263$		

<sup>a</sup>Values for  $\Gamma_p$  computed by combining our  $\Gamma_\gamma$  and  $\Gamma_n$  values with the  $\omega$  values of Druyts *et al.* [13].

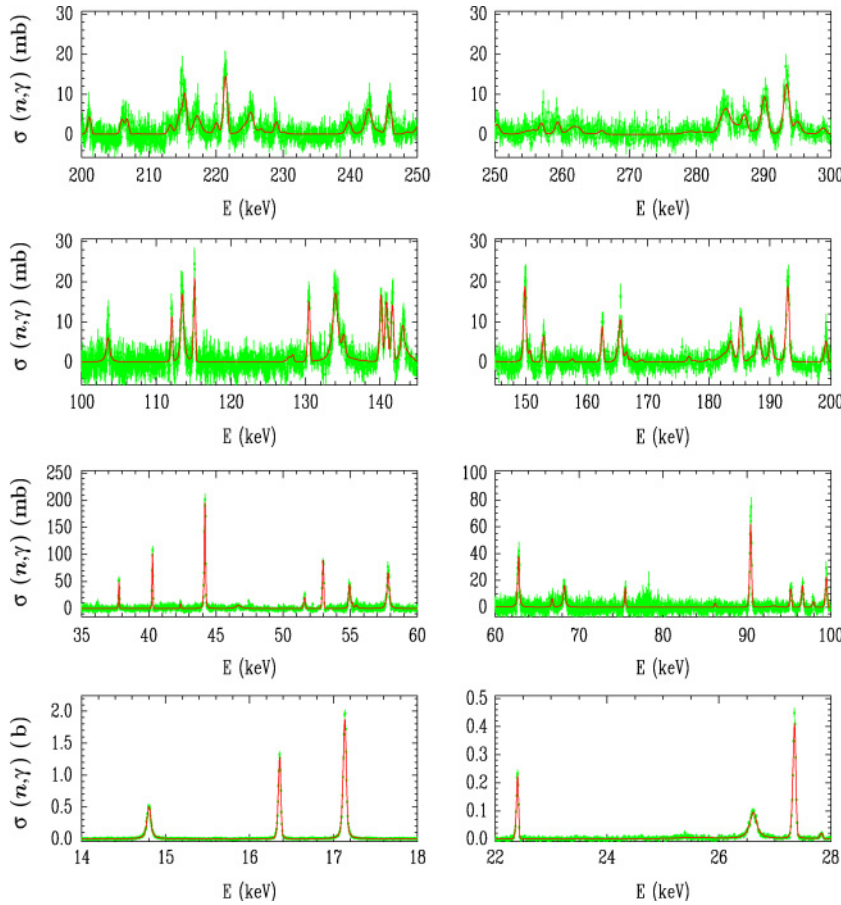


FIG. 7. (Color online) Comparison of SAMMY fits (solid line) to the  $^{nat}\text{Cl}$  capture cross section data of Guber *et al.* [1] for  $14 < E_n < 300$  keV.

performed to obtain final resonance parameters for  $0.1 < E_n < 500$  keV.

From their resonance parameters, Guber *et al.* [1] calculated average cross sections that were rather different from ENDF/B-VI. This difference is very likely the result of underestimated neutron sensitivity in the older measurements as well as an improved calculation of the weighting function.

In Fig. 7, we compare the capture cross section computed from our resonance parameters with the data of Guber *et al.* [1].

In nuclides where the  $(n, \gamma)$  cross section is small, the direct capture (DC) is often a significant fraction of the cross section. Guber *et al.* [1] describe in detail the DC calculations they performed for  $^{35}\text{Cl}$  and  $^{37}\text{Cl}$  using the code TEDCA [21,22]. They calculated that the effect of the DC component was very small for  $^{35}\text{Cl}$ , for which the thermal capture cross section is 43.6 b. However, for  $^{37}\text{Cl}$ , approximately 0.31 b of the thermal capture cross section of 0.433 b is due to direct capture. The parametrized results for the  $^{35,37}\text{Cl}$  DC are given as follows with the cross section in mb and the neutron energy in keV:

$$\sigma_{\text{DC}}(^{35}\text{Cl}) = \frac{0.792 \pm 0.238}{\sqrt{E}} \times (1 + 2.83 \times 10^{-3} E + 2.22 \times 10^{-4} E^2),$$

$$\sigma_{\text{DC}}(^{37}\text{Cl}) = \frac{1.549 \pm 0.811}{\sqrt{E}} \times (1 + 1.57 \times 10^{-6} E + 4.53 \times 10^{-7} E^2).$$

The  $^{35}\text{Cl}$  ( $^{37}\text{Cl}$ ) formula is estimated to be valid up to 10 (100) keV. Below these energy limits, the DC cross section for Cl varies nearly as  $1/v$ . The calculated  $^{35}\text{Cl}$  DC cross section at 10 keV is  $0.26 \pm 0.08$  mb, and the calculated  $^{37}\text{Cl}$  DC cross section at 100 keV is  $0.16 \pm 0.08$  mb. At these upper energy limits, the computed DC values are larger than  $1/v$  by 5% for  $^{35}\text{Cl}$  and by 0.5% for  $^{37}\text{Cl}$ . At higher energies, the DC part is expected to fall off more quickly than  $1/v$  because more and more flux is going into the resonant compound channel. In the DC calculation, this would lead to an imaginary part of the optical neutron potential which increases with energy. However, such an imaginary potential was not considered because the energy dependence is poorly constrained. It can be safely assumed that the DC contribution is negligible about 10 keV (or a few tens of keV) above the given upper limit.

In order to calculate astrophysical  $(n, \gamma)$  rates, Guber *et al.* [1] adjusted their resonance parameters to account for the influence of direct capture. In this paper, we have deduced a set of resonance parameters, including the external level parameters, that reproduce the resonant part of the capture cross section. To this resonant cross section, one must add the DC cross section to obtain the overall capture cross section. It is assumed that there are no interference terms between the direct and resonant components of the capture cross section. The thermal value of the DC cross section is  $0.16 \pm 0.05$  b for  $^{35}\text{Cl}$  and  $0.31 \pm 0.16$  b for  $^{37}\text{Cl}$ .

TABLE III. Cl thermal cross sections and resonance integrals for  $T = 0$  K.

Nuclide <sup>a</sup>	Quantity <sup>b</sup>	ENDF/B-VI <sup>c</sup> (b)	Present evaluation (b)
<sup>35</sup> Cl	$\sigma_{\text{total}}$	$64.70 \pm 0.50$	64.75
	$\sigma_{\text{elastic}}$	$20.60 \pm 0.30$	20.67
	$\sigma_{\gamma}$	$43.60 \pm 0.40$	43.60
	$\sigma_{n,p}$	$0.48 \pm 0.14$	0.480
	$I_{\gamma}$	$17.80 \pm 2.00$	18.19
<sup>37</sup> Cl	$\sigma_{\text{total}}$	$1.583 \pm 0.050$	1.581
	$\sigma_{\text{elastic}}$	$1.150 \pm 0.050$	1.148
	$\sigma_{\gamma}$	$0.433 \pm 0.006$	0.433
	$I_{\gamma}$	$0.204 \pm 0.040$	0.198
	natCl	$\sigma_{\text{total}}$	$49.40 \pm 0.50$
$\sigma_{\text{elastic}}$		$15.90 \pm 0.30$	15.94
$\sigma_{\gamma}$		$33.10 \pm 0.40$	33.14
$\sigma_{n,p}$		$0.36 \pm 0.11$	0.36
$I_{\gamma}$		$13.50 \pm 1.50$	13.83

<sup>a</sup><sup>35</sup>Cl (<sup>37</sup>Cl) abundance = 0.7577 (0.2423).

<sup>b</sup> $\sigma_{\gamma}$  includes the DC cross section.  $I_{\gamma} = \int_{0.5\text{eV}}^{20\text{MeV}} dE\sigma_{\gamma}/E$ .

<sup>c</sup>The ENDF/B-VI values correspond to values quoted in the compilation of Mughabghab *et al.* [15].

#### D. Comparison with ENDF/B-VI

For  $E_n = 0.0253$  eV and  $T = 0$  K, Table III gives a comparison of elastic, capture, ( $n,p$ ), and total cross sections computed from our resonance parameters with the corresponding ENDF/B-VI cross sections, which are based principally on the compilation of Mughabghab [15]. The capture cross section values in Table III include the DC contribution. Agreement between our values and ENDF/B-VI cross sections is excellent for both <sup>35</sup>Cl and <sup>37</sup>Cl. The thermal <sup>35</sup>Cl( $n,p$ ) cross section was discussed in Sec. II B.

Also given in Table III is the resonance capture integral  $I_{\gamma}$ . The  $I_{\gamma}$  values from the present evaluation are in good agreement with the corresponding ENDF/B-VI values, as would be expected from the agreement found for the thermal cross sections.

In Fig. 8, we plot the <sup>35</sup>Cl total cross section for  $T = 300$  K as given by the ENDF/B-VI parameters and by the present evaluation. Between resonances, there are large differences ( $\approx 10\%$  for  $30 \text{ eV} < E_n < 2 \text{ keV}$  and  $\approx 20\%$  for  $2 < E_n < 200 \text{ keV}$ ) between the two calculations. These differences reflect the more accurate recent ORELA transmission measurements. The new ORELA measurements and the older KFK measurements enabled us to extend the resonance parameter representation to 1.2 MeV. The ENDF/B-VI representation above 226 keV is based on Hauser-Feshbach (HF) statistical theory. The latter makes use of energy-averaged transmission coefficients and is therefore expected to only provide average cross sections. High-resolution details can only be included by using our new representation. The HF model predicts average cross section values that are 15–30% lower than the average values from our resonance parameter representation.

#### E. 398- and 4251-eV resonances

The proton widths are significant fractions of the total widths for resonances at 398 and 4251 eV. It was difficult

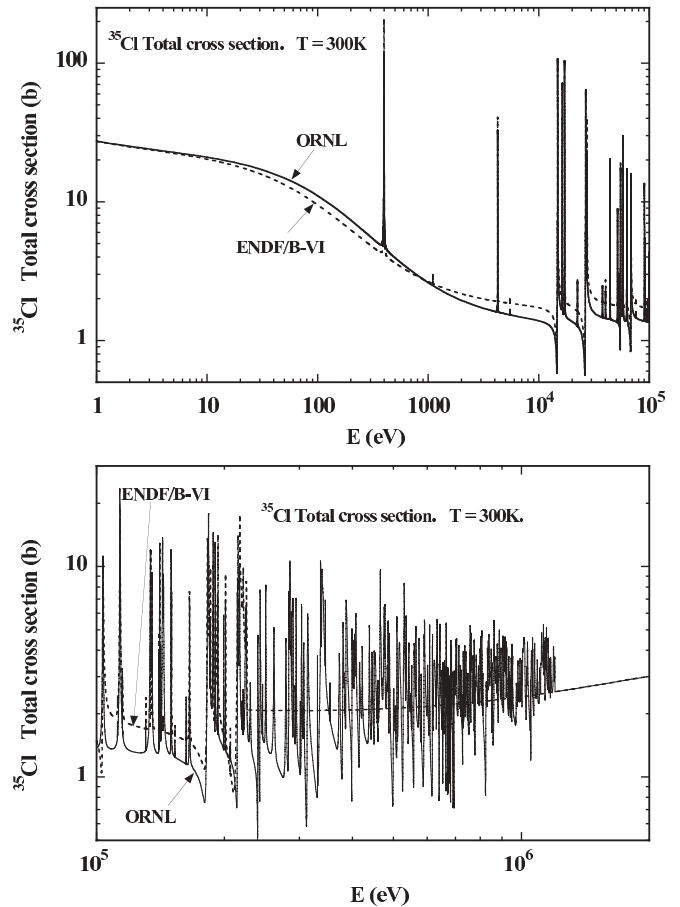


FIG. 8. Comparison of <sup>35</sup>Cl total cross sections from ENDF/B-VI (dashed curve) and the present evaluation (solid curve).

to obtain completely satisfactory fits to all the data for the 398-eV resonance. As shown in Fig. 9, the final proton width, 0.322 eV, gave SAMMY results that are, within uncertainties, consistent with the ORELA capture and transmission data, the <sup>35</sup>Cl( $n,p$ ) data, and the total cross section data of Singh *et al.* [6]. A small error in transmission determination could account for the difference at the peak ( $\sigma_{\text{total}} \approx 100$  b) of the Singh data.

For the 4251-eV resonance, the proton width of 0.230 eV gives good fits to both capture and transmission data as well as a  $g\Gamma_n\Gamma_p/\Gamma$  value that is consistent with the ( $n,p$ ) data.

#### F. Parameter uncertainties and $J^{\pi}$ values

Proton widths were given in Table II for resonances seen in the <sup>35</sup>Cl( $n,p$ ) data. Resonance energies, capture widths, and neutron widths for <sup>35</sup>Cl and <sup>37</sup>Cl are given in Tables IV and V, respectively. Energy and width uncertainties (one standard deviation) are shown in parentheses; e.g., 499.79 (32) indicates  $499.79 \pm 0.32$ . The quoted energy uncertainties include fitting uncertainties taking into account correlations between the energy and width(s) of a particular resonance and correlations between energies of neighboring resonances. To obtain absolute energy uncertainties, one must add in quadrature the uncertainty in the energy scale, which we

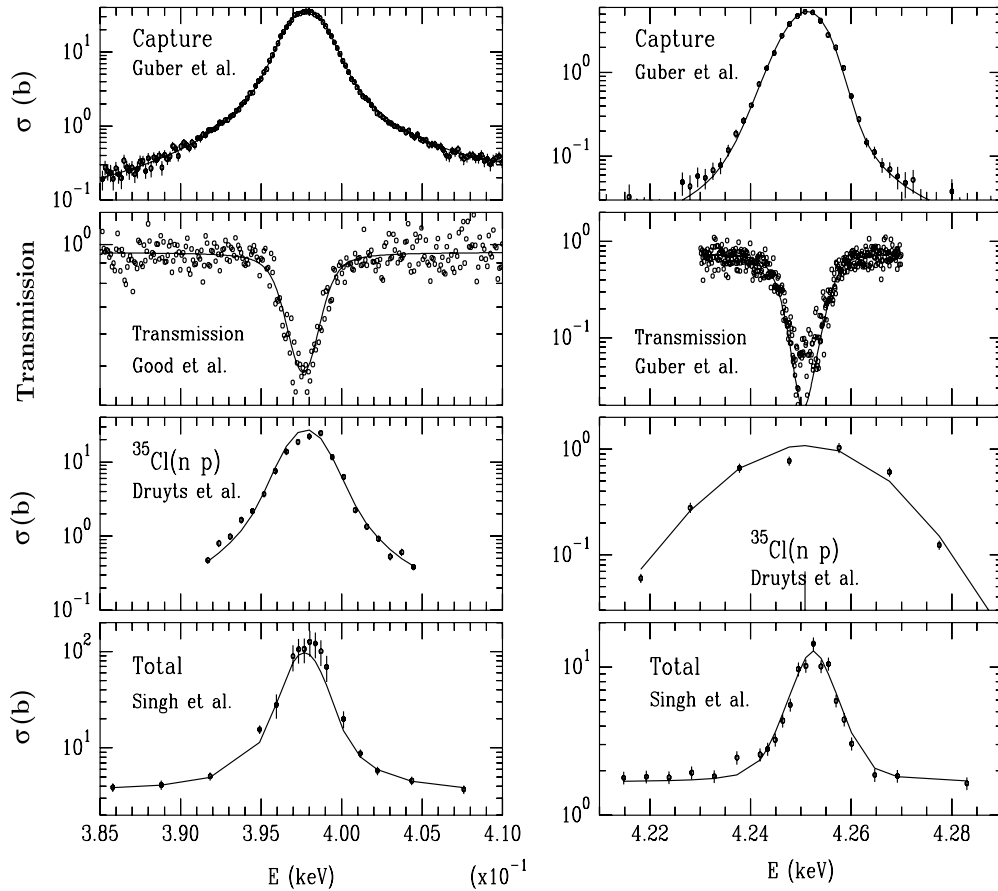


FIG. 9. Comparison of SAMMY fits (solid line) to the  $^{nat}\text{Cl}$  capture and transmission data of Guber *et al.* [1], the transmission data of Good *et al.* [5], the  $^{35}\text{Cl}(n,p)$  data of Druyts *et al.* [13], and the total cross section data of Singh *et al.* [6] for resonances at 398 and 4251 eV.

estimate to be given by

$$(dE)_s = 1.5 \times 10^{-4} E \sqrt{1 + 5.32 \times 10^{-6} E}, \quad (1)$$

where  $(dE)_s$  and  $E$  are in eV. The quoted width uncertainties include both fitting uncertainties and systematic uncertainties related to background, normalization, etc. Correlations between widths were also taken into account. For each resonance, several SAMMY calculations with different width values were performed and overlaid with the data. Both the overlay plots and the changes in  $\chi^2$  with width variation were used to determine final uncertainties that were, in most cases, significantly larger than the SAMMY fit values. For some of the weaker resonances, meaningful uncertainties could not be extracted from the data, and only the width values are quoted.

For resonances above 500 keV, the capture widths were set to the average capture width of the resonances observed in the capture measurements. Average  $^{35}\text{Cl}$  capture widths were 606 MeV for  $s$  waves and 860 MeV for  $p$  waves;  $^{37}\text{Cl}$  values were 416 MeV for  $s$  waves and 488 MeV for  $p$  waves. Both  $^{35}\text{Cl}$  and  $^{37}\text{Cl}$  have ground-state spin  $3/2$  and positive parity. Thus  $s$  waves give two spin groups:  $J^\pi = 1^+$  and  $2^+$ ;  $p$  waves give six spin groups:  $J^\pi = 0^-, 1^-, 2^-$  for channel spin 1 and  $1^-, 2^-, 3^-$  for channel spin 2.

For resonances given tentative  $J^\pi$  assignments in Tables IV and V, we assumed  $l = 0$  or 1. This is a reasonable assumption for most lower energy resonances because the square of the  $d$ -wave reduced neutron width  $\gamma_D$  would correspond to a large fraction of or exceed the Wigner limit  $\hbar^2/Ma_c^2$ . However, for 1-MeV neutrons, the  $^{35}\text{Cl}$  penetrabilities for  $s$ ,  $p$ , and  $d$  waves are 1.030, 0.530, and 0.087, respectively. Thus,  $d$  waves cannot be ruled out for many of the weak, higher energy resonances.

Definite spin and parity assignments in Tables IV and V were made on the basis of detailed shape and intensity analysis in which  $s$ ,  $p$ , and  $d$  waves were considered. A total of 33 new  $J$  assignments were made; parity assignments were made for 15 of these 33 resonances. Characteristic potential-resonant interference patterns were used to identify 16  $s$ -wave resonances in  $^{35}\text{Cl}$  at 14.80, 26.62, 54.93, 68.24, 182.52, 214.92, 242.60, 313.75, 338.98, 386.42, 514.40, 631.04, 640.81, 824.95, 860.96, and 1053.4 keV and five  $s$ -wave resonances in  $^{37}\text{Cl}$  at 8.32, 25.58, 46.65, 93.14, and 136.28 keV. For each of these resonances, the peak cross section allowed definite assignment of either  $J = 1$  or  $J = 2$ . For many other resonances, fits to the data allowed us to both rule out  $s$  waves and to determine spin values. These resonances were identified as  $p$  waves, provided that  $\gamma^2$  was  $\gtrsim 0.10\hbar^2/Ma_c^2$  for  $l = 2$ . For smaller values of  $\gamma^2$ , tentative parity assignments were made.

TABLE IV.  $^{35}\text{Cl}$  resonance parameters. Proton widths are given in Table II. Relative energy uncertainties are quoted. See text.

$E_R$ (keV)	$J^\pi$	$\Gamma_\gamma$ (meV)	$\Gamma_n$ (eV)
-336.93	(2 <sup>-</sup> )	534	38202.
-0.18065	(2 <sup>+</sup> )	530	13.3
0.39782 (2)	2 <sup>-</sup>	665 (46)	0.0505 (20)
4.2508 (1)	1 <sup>-</sup>	472 (25)	0.628 (43)
5.4910 (8)	(1 <sup>-</sup> )	970 (290)	0.0039 (5)
14.802 (1)	2 <sup>+</sup>	346 (24)	32.6 (23)
16.356 (1)	(3 <sup>-</sup> )	387 (15)	5.98 (74)
17.134 (1)	3 <sup>-</sup>	802 (34)	14.1 (13)
22.396 (1)	(0 <sup>-</sup> )	1725 (303)	0.966 (109)
26.616 (2)	2 <sup>+</sup>	304 (32)	115 (11)
27.346 (1)	(2 <sup>-</sup> )	458 (26)	6.03 (113)
37.768 (4)	(1 <sup>-</sup> )	191 (43)	0.441 (166)
40.270 (2)	(3 <sup>-</sup> )	577 (207)	0.177 (27)
44.166 (2)	(1 <sup>-</sup> )	1043 (54)	30.5 (37)
51.608 (5)	(3 <sup>-</sup> )	45 (9)	2.42 (58)
52.974 (3)	(2 <sup>-</sup> )	562 (54)	0.816 (165)
54.932 (3)	1 <sup>+</sup>	367 (55)	46.4 (61)
57.812 (3)	(2 <sup>-</sup> )	538 (76)	107 (14)
62.779 (4)	1 <sup>-</sup>	621 (74)	135 (19)
68.236 (5)	1 <sup>+</sup>	393 (106)	218 (23)
75.495 (17)	(2 <sup>+</sup> )	806	0.080 (25)
90.420 (5)	(2 <sup>-</sup> )	716 (83)	21.8 (37)
90.526 (22)	(2 <sup>-</sup> )	128 (74)	4.24 (203)
95.207 (21)	(3 <sup>-</sup> )	453 (223)	0.155 (53)
96.604 (16)	(0 <sup>-</sup> )	1565 (406)	2.76 (106)
99.441 (13)	(3 <sup>-</sup> )	232 (40)	2.39 (137)
103.52 (1)	1 <sup>-</sup>	388 (133)	382 (57)
112.05 (2)	(3 <sup>-</sup> )	324 (113)	0.264 (75)
113.40 (1)	(2 <sup>-</sup> )	337 (79)	142 (32)
113.61 (1)	(2 <sup>-</sup> )	295 (110)	397 (52)
115.10 (1)	(1 <sup>+</sup> )	739 (135)	4.30 (168)
130.44 (2)	(2 <sup>+</sup> )	759 (210)	0.767 (212)
133.99 (2) <sup>a</sup>	(1 <sup>-</sup> )	2314 (503)	660 (81)
135.12 (1)	1 <sup>(-)</sup>	341 (124)	188 (29)
140.09 (2)	(3 <sup>-</sup> )	366 (89)	3.78 (211)
140.83 (1)	(2 <sup>-</sup> )	546 (93)	98.7 (98)
141.64 (2)	(3 <sup>-</sup> )	313 (83)	3.95 (219)
143.02 (1)	(2 <sup>-</sup> )	492 (145)	315 (30)
149.83 (1)	(2 <sup>-</sup> )	756 (192)	113 (13)
152.92 (4)	(3 <sup>-</sup> )	299 (126)	0.382 (173)
162.56 (4)	(1 <sup>-</sup> )	647 (162)	5.63
165.48 (1)	(1 <sup>-</sup> )	1050 (256)	207 (26)
182.52 (4)	1 <sup>+</sup>	745 (367)	1760 (170)
183.54 (1)	(3 <sup>-</sup> )	333 (113)	462 (41)
185.28 (3)	(3 <sup>-</sup> )	467 (119)	4.48 (246)
188.15 (2)	3 <sup>(-)</sup>	498 (132)	422 (32)
190.18 (1)	(3 <sup>-</sup> )	294 (82)	102 (9)
192.94 (3)	(3 <sup>-</sup> )	756 (139)	16.4 (51)
192.68 (3)	(2 <sup>-</sup> )	229 (102)	33.8 (60)
199.17 (5)	(3 <sup>-</sup> )	255 (90)	2.78 (143)
201.09 (2)	(2 <sup>-</sup> )	291 (106)	36.5 (71)
205.97 (5)	(2 <sup>-</sup> )	451 (246)	0.589 (332)
206.62 (6)	(2 <sup>-</sup> )	594 (322)	0.559 (295)
214.55 (4)	(2 <sup>-</sup> )	232 (122)	42.4 (104)

TABLE IV. (Continued.)

$E_R$ (keV)	$J^\pi$	$\Gamma_\gamma$ (meV)	$\Gamma_n$ (eV)
214.92 (2)	2 <sup>+</sup>	349 (231)	653 (35)
215.35 (5)	(2 <sup>-</sup> )	774 (302)	4.56 (309)
217.10 (2)	2 <sup>(-)</sup>	619 (281)	577 (31)
219.99 (8)	(1 <sup>-</sup> )	400 (241)	3.85
221.39 (3)	(2 <sup>-</sup> )	1593 (438)	4.07 (228)
224.11 (2)	1 <sup>(-)</sup>	403	757 (74)
225.14 (2)	(1 <sup>-</sup> )	1346 (449)	569 (52)
228.89 (8)	(1 <sup>-</sup> )	594 (310)	1.77
230.07 (4)	(0 <sup>-</sup> )	324	812 (136)
239.74 (2)	(1 <sup>+</sup> )	687 (311)	269 (30)
242.60 (2)	2 <sup>+</sup>	902 (261)	344 (28)
243.22 (5)	(0 <sup>-</sup> )	703	217 (64)
245.48 (9)	(0 <sup>-</sup> )	832	6.56
245.85 (6)	(2 <sup>-</sup> )	765 (316)	5.61 (305)
250.20 (2)	2 <sup>(-)</sup>	405 (184)	435 (28)
261.55 (3)	1 <sup>(-)</sup>	846 (498)	1064 (90)
279.11 (3)	1 <sup>(-)</sup>	377	1254 (106)
283.75 (2)	(2 <sup>-</sup> )	647 (307)	424 (37)
284.50 (9)	(1 <sup>-</sup> )	905 (490)	4.16
284.66 (3)	(2 <sup>+</sup> )	499 (367)	1194 (108)
285.61 (3)	(2 <sup>-</sup> )	842 (415)	1569 (135)
287.01 (9)	(2 <sup>-</sup> )	554 (226)	21.3 (88)
290.08 (2)	(2 <sup>-</sup> )	1615 (375)	152 (23)
293.38 (6)	(3 <sup>-</sup> )	1803 (561)	5.94
294.95 (2)	(2 <sup>-</sup> )	739 (310)	475 (37)
301.45 (10)	(2 <sup>-</sup> )	402 (214)	8.86
303.84 (2)	2 <sup>-</sup>	1698 (444)	696 (49)
306.03 (12)	(1 <sup>-</sup> )	563 (342)	7.72
307.41 (3)	1 <sup>(-)</sup>	640	1172 (142)
313.75 (3)	2 <sup>+</sup>	476 (348)	1476 (111)
331.07 (9)	(2 <sup>+</sup> )	398 (247)	32.8 (148)
335.13 (16)	(1 <sup>+</sup> )	358	5526 (910)
336.76 (3)	(3 <sup>-</sup> )	416 (182)	289 (28)
338.98 (3)	2 <sup>+</sup>	2383 (623)	878 (124)
340.70 (19)	1 <sup>-</sup>	565	3875 (760)
341.34 (73)	(0 <sup>-</sup> )	655	5720 (2817)
345.55 (8)	(2 <sup>-</sup> )	348 (206)	63.2 (190)
354.38 (14)	(2 <sup>-</sup> )	233	8.06
372.90 (5)	1 <sup>(-)</sup>	2108 (1118)	1796 (280)
380.26 (6)	(2 <sup>+</sup> )	463	1179 (150)
381.97 (13)	(1 <sup>-</sup> )	8184	1.60 (82)
384.47 (10)	(2 <sup>-</sup> )	5786	1.99 (96)
386.42 (4)	2 <sup>+</sup>	418	1240 (170)
387.89 (12)	(1 <sup>-</sup> )	911 (311)	3239 (240)
399.15 (6)	(1 <sup>+</sup> )	741 (583)	1094 (190)
401.92 (6)	(1 <sup>-</sup> )	333	1212 (191)
404.47 (6)	(1 <sup>-</sup> )	1492 (744)	1010 (159)
407.82 (5)	2 <sup>(-)</sup>	551	2040 (221)
415.67 (21)	(1 <sup>+</sup> )	329	1146 (306)
422.10 (7)	(1 <sup>-</sup> )	2868 (1022)	858 (139)
438.65 (4)	2 <sup>(-)</sup>	645	1274 (143)
444.48 (10)	(2 <sup>-</sup> )	205	181 (43)
450.63 (10)	(1 <sup>+</sup> )	393	461 (168)
451.38 (14)	(2 <sup>-</sup> )	1760 (674)	5.76
452.63 (12)	(1 <sup>-</sup> )	860	3431 (551)

TABLE IV. (Continued.)

$E_R$ (keV)	$J^\pi$	$\Gamma_\gamma$ (meV)	$\Gamma_n$ (eV)
457.89 (15)	(2 <sup>-</sup> )	1147 (725)	7.32
459.36 (17)	(2 <sup>+</sup> )	616	38.6
465.34 (15)	(1 <sup>-</sup> )	367	694 (201)
465.50 (10)	2 <sup>(-)</sup>	558	4040 (308)
469.10 (14)	(2 <sup>-</sup> )	952 (564)	3.76
475.30 (6)	3 <sup>(-)</sup>	830 (541)	2792 (222)
477.20 (17)	(2 <sup>-</sup> )	540	166 (70)
481.28 (35)	(0 <sup>-</sup> )	782	1774
483.69 (21)	(1 <sup>-</sup> )	1907 (1431)	2735 (811)
485.46 (10)	(2 <sup>-</sup> )	1273 (503)	480 (131)
488.63 (8)	(2 <sup>+</sup> )	408	781 (151)
499.79 (32)	(1 <sup>+</sup> )	670	2312 (781)
504.86 (15)	(0 <sup>-</sup> )	860	679 (410)
509.76 (6)	(3 <sup>-</sup> )	860	387 (81)
514.40 (11)	2 <sup>+</sup>	606	5284 (566)
527.94 (8)	(2 <sup>+</sup> )	606	2812 (445)
529.90 (6)	(3 <sup>-</sup> )	860	1354 (159)
535.25 (7)	(3 <sup>-</sup> )	860	448 (63)
542.22 (8)	(1 <sup>+</sup> )	606	522 (210)
543.78 (7)	(2 <sup>-</sup> )	860	692 (142)
547.85 (16)	(0 <sup>-</sup> )	860	764 (365)
552.63 (14)	(1 <sup>-</sup> )	860	279 (109)
559.03 (13)	(2 <sup>+</sup> )	606	1813 (325)
559.25 (22)	(1 <sup>-</sup> )	860	586 (283)
564.58 (7)	(2 <sup>-</sup> )	860	536 (80)
573.88 (8)	(2 <sup>-</sup> )	860	1470 (236)
581.18 (19)	(1 <sup>-</sup> )	860	209 (79)
590.81 (13)	(2 <sup>+</sup> )	606	3236 (342)
590.36 (12)	(2 <sup>-</sup> )	860	755 (186)
591.34 (32)	(1 <sup>-</sup> )	860	167
600.84 (8)	(1 <sup>-</sup> )	860	1209 (194)
608.06 (7)	(3 <sup>-</sup> )	860	775 (125)
614.26 (10)	(1 <sup>-</sup> )	860	1153 (213)
618.10 (7)	(2 <sup>-</sup> )	860	1075 (146)
621.68 (14)	(2 <sup>+</sup> )	606	6759 (796)
629.58 (27)	(1 <sup>-</sup> )	860	623 (201)
631.04 (11)	2 <sup>+</sup>	606	1637 (325)
633.10 (23)	(2 <sup>-</sup> )	860	145 (83)
640.81 (7)	2 <sup>+</sup>	606	860 (160)
642.74 (10)	(2 <sup>-</sup> )	860	950 (145)
654.21 (12)	(1 <sup>+</sup> )	606	519 (143)
657.81 (25)	(2 <sup>+</sup> )	606	207 (133)
659.35 (30)	(1 <sup>-</sup> )	860	136
665.29 (25)	(1 <sup>+</sup> )	606	141 (97)
665.80 (15)	(3 <sup>-</sup> )	860	210 (41)
672.36 (15)	(1 <sup>+</sup> )	606	575 (138)
673.98 (27)	(3 <sup>-</sup> )	606	49.0
678.00 (32)	(1 <sup>+</sup> )	606	133
681.06 (12)	(2 <sup>+</sup> )	606	665 (123)
681.67 (29)	(3 <sup>-</sup> )	860	60.3
685.02 (24)	(3 <sup>-</sup> )	860	117 (48)
690.27 (10)	(2 <sup>+</sup> )	606	463 (121)
694.94 (8)	(1 <sup>+</sup> )	606	1825 (270)
701.00 (10)	(3 <sup>-</sup> )	860	1252 (167)
703.62 (15)	(2 <sup>-</sup> )	860	931 (198)

TABLE IV. (Continued.)

$E_R$ (keV)	$J^\pi$	$\Gamma_\gamma$ (meV)	$\Gamma_n$ (eV)
712.53 (9)	2 <sup>(-)</sup>	860	3301 (318)
718.38 (17)	(1 <sup>-</sup> )	860	974 (188)
721.99 (15)	(1 <sup>-</sup> )	860	827 (176)
725.18 (32)	(1 <sup>+</sup> )	606	167
729.58 (14)	(2 <sup>-</sup> )	860	647 (114)
732.89 (23)	(1 <sup>-</sup> )	860	1956 (438)
735.01 (18)	(2 <sup>-</sup> )	860	378 (109)
739.81 (10)	2 <sup>(-)</sup>	860	3042 (359)
748.48 (19)	(1 <sup>-</sup> )	860	1024 (226)
754.69 (19)	(1 <sup>+</sup> )	606	2691 (797)
757.46 (12)	3 <sup>(-)</sup>	860	3780 (330)
761.11 (13)	3 <sup>(-)</sup>	860	2239 (428)
765.41 (25)	(1 <sup>-</sup> )	860	1520 (532)
770.29 (10)	(2 <sup>-</sup> )	860	3185 (390)
774.97 (19)	(3 <sup>-</sup> )	860	369 (89)
779.97 (21)	(2 <sup>+</sup> )	606	5311 (914)
781.46 (23)	(1 <sup>+</sup> )	606	1294 (713)
792.78 (17)	(1 <sup>-</sup> )	860	1041 (219)
798.56 (18)	(2 <sup>-</sup> )	860	2911 (449)
801.33 (21)	(2 <sup>-</sup> )	860	681 (207)
806.88 (12)	(3 <sup>-</sup> )	860	630 (92)
810.34 (26)	(1 <sup>-</sup> )	860	509 (155)
824.95 (13)	2 <sup>+</sup>	606	2764 (623)
827.38 (33)	(2 <sup>-</sup> )	606	436 (210)
831.58 (48)	(1 <sup>+</sup> )	860	445
832.26 (26)	(2 <sup>-</sup> )	860	1383 (348)
835.85 (31)	(2 <sup>-</sup> )	860	1181 (343)
838.95 (23)	(3 <sup>-</sup> )	860	3395 (503)
845.15 (32)	(1 <sup>-</sup> )	860	4177 (1014)
848.41 (14)	(2 <sup>-</sup> )	860	2391 (533)
852.49 (11)	(2 <sup>-</sup> )	860	1727 (327)
860.96 (17)	2 <sup>+</sup>	606	7202 (1238)
862.61 (14)	(3 <sup>-</sup> )	860	695 (181)
871.57 (13)	(1 <sup>-</sup> )	860	1987 (338)
876.99 (14)	(2 <sup>-</sup> )	860	576 (144)
882.98 (15)	(1 <sup>+</sup> )	606	978 (391)
886.58 (14)	(3 <sup>-</sup> )	860	3198 (344)
895.07 (11)	(2 <sup>-</sup> )	860	1506 (223)
905.86 (24)	(3 <sup>-</sup> )	860	441 (108)
910.90 (16)	(3 <sup>-</sup> )	860	3339 (446)
915.65 (24)	(2 <sup>-</sup> )	860	1034 (372)
922.52 (14)	(2 <sup>-</sup> )	860	1572 (274)
933.14 (13)	(2 <sup>-</sup> )	860	939 (151)
936.66 (15)	(1 <sup>-</sup> )	860	606 (195)
943.95 (15)	(1 <sup>-</sup> )	860	556 (204)
946.10 (14)	(2 <sup>-</sup> )	860	481 (152)
950.47 (12)	(3 <sup>-</sup> )	860	645 (112)
953.35 (13)	(2 <sup>-</sup> )	860	1001 (191)
974.75 (39)	(1 <sup>-</sup> )	860	3259 (845)
981.04 (26)	(2 <sup>-</sup> )	860	4229 (692)
984.51 (47)	(1 <sup>-</sup> )	860	1802 (530)
991.54 (18)	(2 <sup>-</sup> )	860	4348 (744)
999.85 (12)	(2 <sup>-</sup> )	860	3022 (363)
1006.5 (3)	(2 <sup>-</sup> )	860	3591 (1470)
1010.4 (4)	(3 <sup>-</sup> )	860	7910 (1260)

TABLE IV. (Continued.)

$E_R$ (keV)	$J^\pi$	$\Gamma_\gamma$ (meV)	$\Gamma_n$ (eV)
1016.5 (3)	(2 <sup>-</sup> )	860	4020 (835)
1028.5 (3)	(2 <sup>-</sup> )	860	2389 (495)
1033.7 (2)	(3 <sup>-</sup> )	860	3550 (484)
1050.6 (2)	(2 <sup>-</sup> )	860	1304 (323)
1053.4 (4)	2 <sup>+</sup>	606	2038 (609)
1055.5 (4)	(2 <sup>-</sup> )	860	3889 (701)
1062.1 (4)	(3 <sup>-</sup> )	860	421 (108)
1071.2 (3)	(3 <sup>-</sup> )	860	1944 (282)
1074.0 (4)	(2 <sup>-</sup> )	860	1039 (349)
1080.2 (4)	(2 <sup>-</sup> )	860	751 (250)
1085.4 (7)	(3 <sup>-</sup> )	860	134
1088.7 (3)	(2 <sup>-</sup> )	860	5239 (1086)
1092.0 (5)	(1 <sup>-</sup> )	860	1975 (632)
1103.7 (2)	(3 <sup>-</sup> )	860	1609 (160)
1109.2 (4)	(1 <sup>+</sup> )	606	2742 (1033)
1115.7 (3)	(2 <sup>-</sup> )	860	3444 (738)
1116.0 (9)	(2 <sup>-</sup> )	860	43637 (4416)
1120.9 (5)	(3 <sup>-</sup> )	860	389 (145)
1126.9 (4)	(3 <sup>-</sup> )	860	616 (164)
1132.0 (3)	(2 <sup>-</sup> )	860	1523 (389)
1137.9 (3)	(2 <sup>+</sup> )	606	1836 (473)
1138.7 (6)	(1 <sup>-</sup> )	860	954 (524)
1144.9 (3)	(3 <sup>-</sup> )	860	1587 (293)
1155.3 (2)	(3 <sup>-</sup> )	860	1578 (229)
1165.3 (2)	(2 <sup>-</sup> )	860	7310 (827)
1172.1 (3)	(2 <sup>-</sup> )	860	1495 (430)
1177.0 (4)	(1 <sup>-</sup> )	860	1488 (574)
1189.7 (2)	(3 <sup>-</sup> )	860	7290 (778)
1198.5 (2)	(2 <sup>-</sup> )	860	3243 (659)
1205.7	(1 <sup>+</sup> )	606	643
1209.0	(3 <sup>-</sup> )	860	3485
1218.1	(2 <sup>-</sup> )	860	3247
1225.3	(1 <sup>-</sup> )	860	1807
1237.2	(3 <sup>-</sup> )	860	5888
1243.5	(2 <sup>-</sup> )	860	3097
1257.7	(2 <sup>+</sup> )	606	1750
1268.6	(3 <sup>-</sup> )	860	2391
1277.7	(3 <sup>-</sup> )	860	2984
1283.8	(2 <sup>-</sup> )	860	5041
1311.8	(2 <sup>-</sup> )	860	795
1315.1	(3 <sup>-</sup> )	860	12106
1337.1	(2 <sup>-</sup> )	860	4850
1353.6	(1 <sup>-</sup> )	860	38797
1354.1	(2 <sup>-</sup> )	860	11033
1366.1	(2 <sup>-</sup> )	860	8350
1390.7	(3 <sup>-</sup> )	860	5502
1403.9	(2 <sup>-</sup> )	860	8067
1425.4	(3 <sup>-</sup> )	860	13820
1434.3	(2 <sup>-</sup> )	860	5423
1435.5	(1 <sup>-</sup> )	860	5366
1441.4	(2 <sup>-</sup> )	860	1609
1485.1	(3 <sup>-</sup> )	860	10541
7563.1	(2 <sup>+</sup> )	384	621905

<sup>a</sup>May be a doublet.TABLE V. <sup>37</sup>Cl resonance parameters Relative energy uncertainties are quoted. See text.

$E_R$ (keV)	$J^\pi$	$\Gamma_\gamma$ (meV)	$\Gamma_n$ (eV)
-1.0000	(1 <sup>+</sup> )	225	9.56
8.3208 (30)	2 <sup>+</sup>	196 (23)	78.7 (48)
25.579 (14)	1 <sup>+</sup>	513 (123)	652 (68)
27.824 (2)	(2 <sup>-</sup> )	79 (26)	5.54 (156)
32.187 (3)	(1 <sup>-</sup> )	82 (23)	10.5 (29)
42.358 (19)	(1 <sup>-</sup> )	260 (154)	0.279 (138)
46.653 (10)	2 <sup>+</sup>	265 (95)	390 (48)
51.548 (11)	(3 <sup>-</sup> )	78 (38)	3.33 (156)
55.146 (28)	(0 <sup>-</sup> )	70	3.92
55.440 (3)	2 <sup>-</sup>	179 (67)	123 (26)
66.707 (7)	(2 <sup>-</sup> )	107 (62)	25.9 (58)
66.837 (5)	(2 <sup>-</sup> )	154 (74)	50.9 (106)
86.211 (36)	(1 <sup>-</sup> )	252	1.10
93.138 (14)	2 <sup>+</sup>	221 (86)	727 (110)
97.901 (36)	(1 <sup>+</sup> )	707 (350)	1.45 (87)
114.74 (5)	(0 <sup>-</sup> )	331	250 (116)
125.26 (2)	(3 <sup>-</sup> )	6	31.1 (82)
125.51 (2)	(3 <sup>-</sup> )	6	26.4 (72)
127.76 (1)	(2 <sup>+</sup> )	268 (158)	391 (70)
128.22 (4)	(1 <sup>-</sup> )	281 (139)	35.5
135.43 (7)	(0 <sup>-</sup> )	238	164 (109)
136.28 (3)	2 <sup>+</sup>	262	1392 (242)
143.72 (2)	(3 <sup>-</sup> )	171 (100)	653 (107)
144.34 (5)	(1 <sup>-</sup> )	154 (90)	64.1 (322)
150.08 (4)	(1 <sup>-</sup> )	515 (303)	89.6 (405)
150.67 (5)	(2 <sup>-</sup> )	412 (185)	12.7 (73)
157.56 (2)	(2 <sup>-</sup> )	166	149 (26)
164.95 (8)	(0 <sup>-</sup> )	1176	215 (140)
166.47 (4)	(1 <sup>-</sup> )	827 (397)	86.6 (313)
167.30 (6)	(1 <sup>-</sup> )	286	51.5 (256)
168.96 (2)	(2 <sup>-</sup> )	151	248 (50)
176.72 (2)	(2 <sup>-</sup> )	361 (199)	166 (28)
177.61 (10)	(0 <sup>-</sup> )	488	459 (227)
179.86 (6)	(1 <sup>+</sup> )	216	1610 (297)
179.91 (5)	(1 <sup>-</sup> )	216	117 (34)
187.00 (2)	(2 <sup>+</sup> )	318	309 (60)
190.70 (8)	(1 <sup>+</sup> )	464	1111 (269)
191.13 (5)	(1 <sup>-</sup> )	392	184 (64)
208.35 (3)	(1 <sup>+</sup> )	115	519 (132)
213.23 (7)	(1 <sup>-</sup> )	1277 (671)	25.9 (149)
214.16 (13)	(0 <sup>-</sup> )	1718	271 (163)
217.68 (12)	(0 <sup>-</sup> )	3104	431 (250)
218.66 (11)	(0 <sup>-</sup> )	358	151 (95)
219.68 (11)	(0 <sup>-</sup> )	356	107 (62)
221.15 (4)	(2 <sup>+</sup> )	201	65.2 (178)
226.56 (10)	(1 <sup>+</sup> )	477	4.30
227.66 (10)	(0 <sup>-</sup> )	919	44.3 (303)
229.90 (13)	(0 <sup>-</sup> )	241	249 (120)
244.09 (9)	(3 <sup>-</sup> )	235	23.0 (103)
248.45 (4)	(2 <sup>+</sup> )	267	133 (37)
254.03 (2)	2 <sup>(-)</sup>	366	694 (87)
254.78 (10)	(1 <sup>-</sup> )	548	64.0 (304)
255.66 (8)	(1 <sup>-</sup> )	876	60.4 (258)

TABLE V. (Continued.)

$E_R$ (keV)	$J^\pi$	$\Gamma_\gamma$ (meV)	$\Gamma_n$ (eV)
256.78 (7)	(1 <sup>+</sup> )	2384 (1194)	41.8 (175)
259.25 (7)	(2 <sup>-</sup> )	1636 (799)	43.3 (169)
262.44 (6)	(2 <sup>-</sup> )	577	73.1 (322)
263.86 (13)	(0 <sup>-</sup> )	365	186 (122)
265.84 (11)	(1 <sup>-</sup> )	917	65.7 (290)
278.12 (19)	(0 <sup>-</sup> )	362	109
280.66 (8)	(2 <sup>-</sup> )	302	92.8 (355)
281.52 (8)	(1 <sup>+</sup> )	318	132 (47)
288.35 (11)	(3 <sup>-</sup> )	359	36.8 (195)
298.77 (12)	(3 <sup>-</sup> )	818 (522)	13.6
301.17 (9)	(1 <sup>-</sup> )	376	401 (118)
308.95 (9)	(1 <sup>-</sup> )	332	515 (197)
311.06 (7)	(2 <sup>-</sup> )	349	2369 (366)
316.61 (20)	(1 <sup>+</sup> )	369	112
333.29 (8)	(3 <sup>-</sup> )	365	239 (78)
334.08 (16)	(1 <sup>+</sup> )	366	1037 (372)
336.00 (23)	(1 <sup>-</sup> )	358	790 (497)
358.38 (12)	(2 <sup>+</sup> )	218	764 (270)
360.74 (12)	(2 <sup>-</sup> )	338	197 (84)
368.40 (14)	(2 <sup>-</sup> )	332	98 (55)
377.17 (87)	(0 <sup>-</sup> )	945	3368 (2407)
379.39 (12)	(3 <sup>-</sup> )	383	870 (206)
383.65 (14)	(2 <sup>-</sup> )	841	2132 (719)
391.89 (17)	(2 <sup>-</sup> )	383	84
394.43 (22)	(1 <sup>+</sup> )	384	64
411.72 (18)	(2 <sup>-</sup> )	361	213 (108)
414.24 (61)	(1 <sup>-</sup> )	352	3035 (1331)
415.19 (28)	(2 <sup>-</sup> )	336	921 (513)
417.05 (19)	(2 <sup>-</sup> )	349	229 (110)
417.86 (20)	(2 <sup>-</sup> )	351	3150 (892)
424.04 (15)	(3 <sup>-</sup> )	374	328 (118)
425.18 (16)	(2 <sup>-</sup> )	347	603 (208)
427.53 (16)	(3 <sup>-</sup> )	1056	150 (79)
431.03 (18)	(2 <sup>+</sup> )	258	144 (83)
434.21 (21)	(2 <sup>+</sup> )	356	95
435.89 (23)	(2 <sup>-</sup> )	397	153 (108)
446.39 (13)	(3 <sup>-</sup> )	470	2215 (460)
491.52 (64)	(1 <sup>-</sup> )	325	3532 (2276)
493.46 (64)	(2 <sup>+</sup> )	325	269
495.70 (31)	(2 <sup>-</sup> )	325	507 (284)
498.14 (45)	(2 <sup>-</sup> )	1440	2134 (1087)
500.36 (51)	(2 <sup>-</sup> )	404	1754 (1027)
507.97 (20)	(1 <sup>+</sup> )	416	3127 (2285)
513.60 (33)	(1 <sup>-</sup> )	488	197
516.62 (18)	(2 <sup>-</sup> )	488	1078 (551)
523.39 (20)	(1 <sup>-</sup> )	488	939 (497)
525.73 (11)	(3 <sup>-</sup> )	488	858 (231)
553.89 (28)	(1 <sup>-</sup> )	488	1967 (942)
557.17 (18)	(2 <sup>-</sup> )	488	794 (277)
569.51 (31)	(1 <sup>-</sup> )	488	477 (325)
571.44 (79)	(0 <sup>-</sup> )	488	1072
576.36 (29)	(2 <sup>-</sup> )	488	1108 (640)
578.39 (30)	(1 <sup>-</sup> )	488	1372 (855)
584.89 (24)	(1 <sup>-</sup> )	488	697 (333)
586.87 (71)	(0 <sup>-</sup> )	488	844

TABLE V. (Continued.)

$E_R$ (keV)	$J^\pi$	$\Gamma_\gamma$ (meV)	$\Gamma_n$ (eV)
588.40 (19)	(3 <sup>-</sup> )	488	644 (229)
596.99 (33)	(1 <sup>-</sup> )	488	574
603.98 (25)	(1 <sup>-</sup> )	488	1054 (586)
606.03 (65)	(0 <sup>-</sup> )	488	1029
610.42 (37)	(2 <sup>-</sup> )	488	1386 (519)
611.81 (42)	(1 <sup>+</sup> )	416	681 (436)
627.24 (32)	(2 <sup>+</sup> )	416	912 (519)
634.68 (40)	(2 <sup>-</sup> )	488	922 (550)
636.77 (28)	(3 <sup>-</sup> )	488	833 (386)
649.61 (13)	(2 <sup>+</sup> )	416	2017 (685)
651.84 (20)	(2 <sup>-</sup> )	488	66
670.19 (24)	(2 <sup>+</sup> )	416	616 (220)
693.38 (42)	(2 <sup>-</sup> )	488	231 (150)
708.42 (24)	(3 <sup>-</sup> )	488	1044 (342)
742.45 (42)	(2 <sup>-</sup> )	488	465 (362)
747.62 (40)	(2 <sup>+</sup> )	416	299
789.29 (40)	(2 <sup>+</sup> )	416	262
820.59 (18)	(3 <sup>-</sup> )	488	3126 (826)
865.90 (19)	(2 <sup>-</sup> )	488	6575 (3198)
890.16 (17)	(2 <sup>-</sup> )	488	1235 (583)
899.99 (17)	(2 <sup>-</sup> )	488	571 (301)
919.00 (17)	(1 <sup>-</sup> )	488	997
925.24 (98)	(3 <sup>-</sup> )	488	402 (268)
926.96 (63)	(2 <sup>-</sup> )	488	1458 (653)
942.19 (17)	(1 <sup>-</sup> )	488	940 (543)
958.82 (18)	(2 <sup>-</sup> )	488	1138 (351)
962.41 (16)	(3 <sup>-</sup> )	488	1255 (392)
967.39 (13)	(2 <sup>-</sup> )	488	1209 (416)
970.67 (14)	(3 <sup>-</sup> )	488	1805 (664)
995.44 (15)	(2 <sup>-</sup> )	488	2934 (1520)
1024.2 (3)	(2 <sup>-</sup> )	488	2600 (1110)
1038.0 (3)	(2 <sup>-</sup> )	488	2262 (1240)
1044.1 (3)	(2 <sup>-</sup> )	488	1683 (761)
1083.3 (6)	(2 <sup>+</sup> )	416	1641
1098.5 (3)	(2 <sup>-</sup> )	488	1527 (582)
1214.9	(2 <sup>-</sup> )	488	4254
1292.7	(2 <sup>-</sup> )	488	4327
1304.4	(3 <sup>-</sup> )	488	12935
1386.8	(3 <sup>-</sup> )	488	29158
1482.1	(2 <sup>+</sup> )	416	7118
1809.6	(1 <sup>+</sup> )	384	303262

An example of the  $J^\pi$  analysis is given in Fig. 10, where we plot the ORELA <sup>nat</sup>Cl total cross section data and SAMMY fits for three  $J^\pi$  values for the 408-keV <sup>35</sup>Cl resonance. The other possible  $J^\pi$  values, 1<sup>+</sup> and 1<sup>-</sup>, gave much poorer fits to the data. Although an acceptable fit can be obtained with a 2<sup>+</sup>d-wave resonance, we consider that possibility unlikely because  $\gamma_D^2$  would exhaust 4.6% of the Wigner limit. Nonetheless, we have assigned a tentative negative parity value in Table IV, i.e.,  $J^\pi = 2^{(-)}$ . Below 160 keV, the capture results reported by Macklin [23] for a sample enriched to 98.2% in <sup>37</sup>Cl were utilized for the identification of several resonances

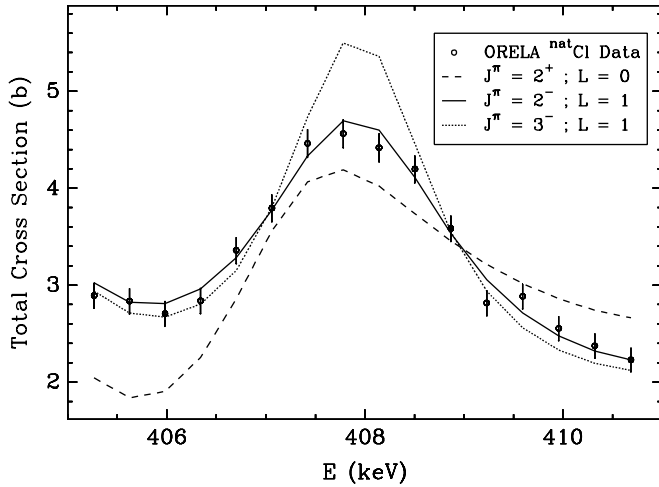


FIG. 10. Comparison of SAMMY fits for three  $J^\pi$  values with ORELA  $^{nat}\text{Cl}$  total cross section data for the 408-keV resonance in  $^{35}\text{Cl}$ .

belonging to  $^{37}\text{Cl}$ . Isotopic assignments for higher energy resonances were based on intensity analysis utilizing the 3/1 relative abundance of  $^{35}\text{Cl}/^{37}\text{Cl}$ .

### III. AVERAGE QUANTITIES

Ideally, the distribution of neutron widths corresponding to a particular spin group, e.g.,  $J^\pi = 2^+$ , is expected to follow the hypothesis of Porter and Thomas [24], and the nearest neighbor level spacings are expected to be apportioned according to the Wigner distribution [25]. The distribution of  $J = 2$ ,  $s$ -wave  $^{35}\text{Cl}$  neutron widths in the energy range  $0 < E_n < 1$  MeV is compared with the Porter-Thomas distribution in Fig. 11. The agreement is quite good, considering that there are only 27 resonances. For the energy range  $0 < E_n < 1$  MeV, the

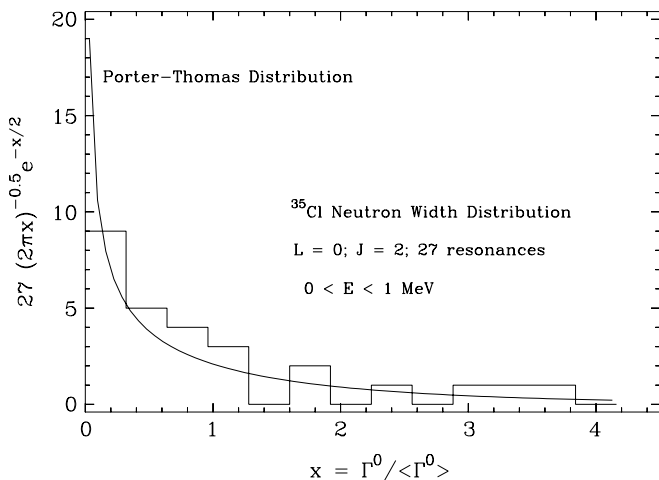


FIG. 11. Comparison of the neutron width distribution with the Porter-Thomas distribution for  $J = 2$ ,  $s$ -wave  $^{35}\text{Cl}$  resonances.

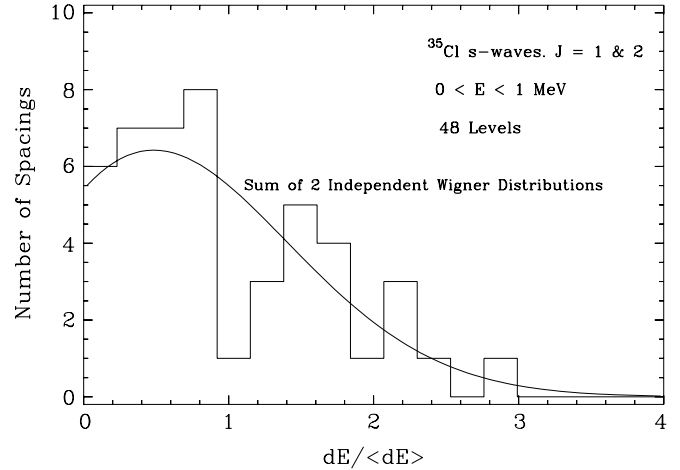


FIG. 12. Comparison of the level spacing distribution with the Wigner distribution for  $^{35}\text{Cl}$   $s$ -wave resonances. The curve is the sum of two uncorrelated Wigner distributions corresponding to resonances with  $J = 1, 2$ .

distribution of nearest-neighbor level spacings is shown in Fig. 12 for the 48  $^{35}\text{Cl}$  resonances identified as  $s$  wave. Also shown is the sum of two uncorrelated Wigner distributions [26] normalized so that the area under the curve is the total number of level spacings. Some of the resonances tentatively identified as  $s$  wave are rather weak; therefore, we conclude that the approximate agreement with the Wigner distribution is reasonable.

#### A. Level spacing

In Fig. 13, we plot the cumulative number of resonances vs neutron energy for both  $s$  and  $p$  waves. The lines are unweighted fits to the data. In the plots, the solid symbols and solid lines correspond to inclusion of all resonances, some of which are very narrow and whose  $l$  and  $J$  values are very uncertain because of experimental resolution, background conditions, and nearby stronger resonances. Some of these weak resonances are in all likelihood  $d$  waves; most are in energy regions where the cumulative number departs significantly from linearity as a function of  $E$ . When the very weak  $^{35}\text{Cl}$  resonances (neutron reduced widths  $\lesssim 0.1$  eV) are removed, the open symbols and dashed lines are obtained so that the behavior is much closer to that expected from purely statistical considerations. Of course, the very narrow resonances do not affect the strength functions appreciably. In Table VI, we give average neutron and capture widths for  $0 < E < 500$  keV; also given are the average level spacings  $\langle D_l \rangle \equiv (E_f - E_i)/(N^{\text{obs}} - 1)$ , where  $E_i$  and  $E_f$  are the energies of the first and last resonances and  $N^{\text{obs}}$  is the number of resonances observed. No corrections were made for missing levels. Our average capture widths are consistent with values for other nuclei in this mass region. For  $s$  waves,  $\langle \Gamma_\gamma \rangle = 1.0 \pm 0.6$  eV for  $^{34}\text{S}$  [27] and  $1.5 \pm 0.9$  eV for  $^{40}\text{Ca}$  [15]. Similarly, for  $p$  waves,  $\langle \Gamma_\gamma \rangle = 1.2 \pm 0.3$  eV for  $^{34}\text{S}$  [27] and  $0.36 \pm 0.09$  eV for  $^{40}\text{Ca}$  [15].

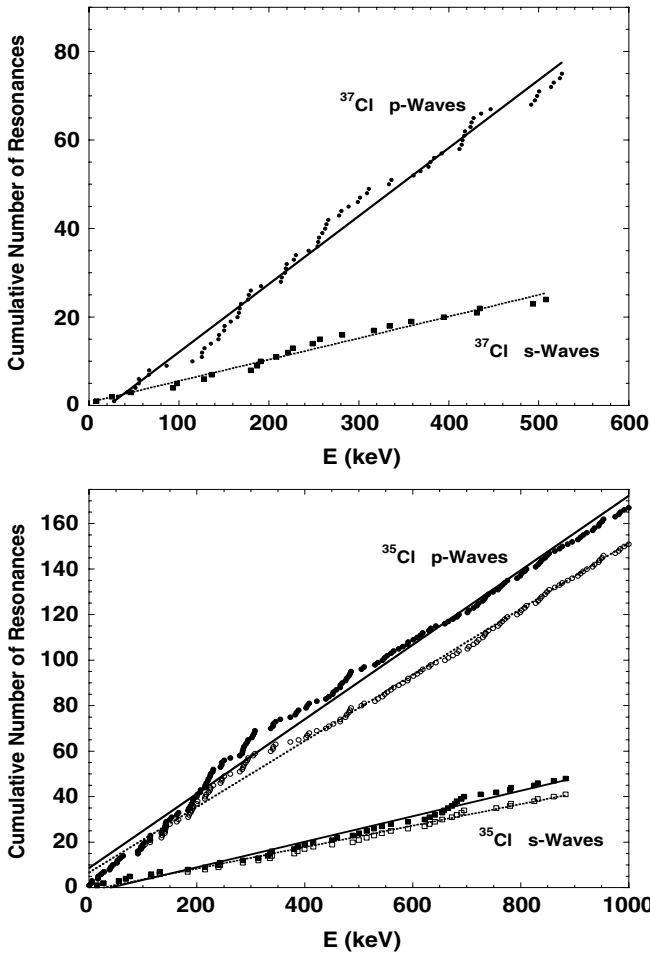


FIG. 13. Cumulative number of *s*- and *p*-wave resonances vs *E* for <sup>35</sup>Cl (lower) and <sup>37</sup>Cl (upper); *s* waves are plotted as squares and *p* waves as circles. The lines are unweighted fits. The open symbols and dashed lines for <sup>35</sup>Cl were obtained by removing very weak resonances (neutron reduced widths  $\lesssim 0.1$  eV).

**B. Strength functions**

Neutron strength functions were determined by unweighted least-squares fits to the cumulative reduced width vs energy, as shown in Fig. 14. The slopes of the lines give the strength functions directly. This procedure yielded values consistent with those computed from the conventional relation

$$S_l = \frac{1}{(2l + 1)\Delta E} \sum g_j \Gamma_{nj}^l,$$

TABLE VI. Average widths and level spacings for <sup>35,37</sup>Cl.

Nuclide	<i>l</i>	$\langle \Gamma_n \rangle^a$ (eV)	$\langle \Gamma_\gamma \rangle^a$ (eV)	$\langle D_l \rangle^b$ (keV)	<i>E<sub>f</sub></i> (keV)	<i>N<sup>obs</sup></i>
<sup>35</sup> Cl	0	867 (55)	0.61 (7)	22.0 (20)	1053.4	48
	1	547 (37)	0.86 (11)	6.1 (05)	1050.6	173
<sup>37</sup> Cl	0	444 (34)	0.42 (8)	22.0 (30)	493.5	23
	1	515 (60)	0.49 (7)	6.9 (05)	498.1	69

<sup>a</sup> $\langle \Gamma_n \rangle$  and  $\langle \Gamma_\gamma \rangle$  are calculated for  $0 < E < 500$  keV.

<sup>b</sup> $\langle D_l \rangle \equiv (E_f - E_i)/(N^{obs} - 1)$ .

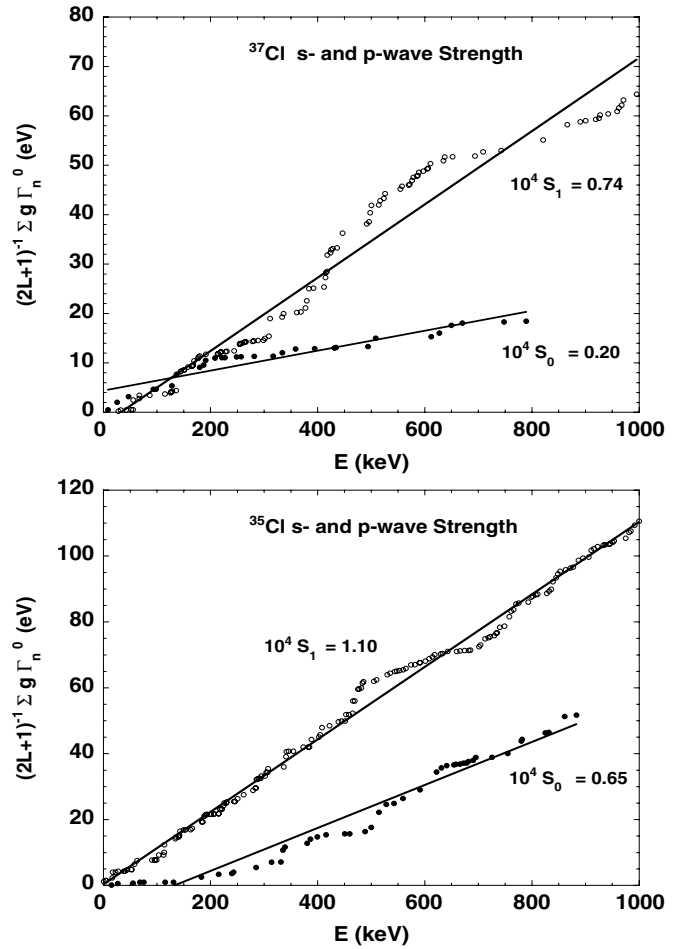


FIG. 14. Cumulative reduced width vs *E* for <sup>35</sup>Cl (lower) and <sup>37</sup>Cl (upper); *s* waves are plotted as solid symbols and *p* waves as open symbols. The lines are unweighted fits.

where  $\Delta E$  is the energy interval,  $g_j$  is the statistical factor, and the reduced neutron width is given by

$$\Gamma_{nj}^l = \sqrt{\frac{1 \text{ eV}}{E_o} \frac{\rho}{P_l}} \Gamma_{nj}.$$

$E_o$  is the resonance energy,  $P_l$  is the penetrability, and  $\rho = ka$ , where  $k$  is the wave number and  $a$  the nuclear radius. The statistical uncertainty in the strength function is  $S_l \sqrt{2/N}$ , where  $N$  is the number of resonances.

Our *p*-wave results are the first reported values of  $S_1$  for the Cl nuclides. Our Cl values are consistent with values for the neighboring nuclides <sup>34</sup>S [27] and <sup>39</sup>K [15]:  $10^4 S_1 = 0.9 \pm 0.3$  and  $1.0 \pm 0.3$ , respectively.

We compare our strength functions with previous results in Table VII. Corrections to the  $S_l$  for resonances too narrow to be observed are estimated to be much smaller than the quoted uncertainties. However, incorrect angular momentum assignments can affect strength values dramatically. For <sup>37</sup>Cl, Mughaghab *et al.* [15] quote a value of  $10^4 S_0 = 0.70 \pm 0.27$  for  $0 < E_n < 202$  keV; this included 145- and 202-keV resonances. We assign the 145-keV resonance to <sup>35</sup>Cl, and we do not see a 202-keV resonance. Without these resonances,

TABLE VII. Strength functions from the present work compared with previous values.

Nuclide	$l$	Present work			Mughaghab <i>et al.</i> [15]			RIPL-2 [28]
		$\Delta E$ (keV)	Number of resonances	$10^4 S_l$	$\Delta E$ (keV)	Number of resonances	$10^4 S_0$	$10^4 S_0$
$^{35}\text{Cl}$	0	1000	48	$0.65 \pm 0.13$	200	11	$0.38 \pm 0.16$	$0.33 \pm 0.15$
	1	1000	167	$1.10 \pm 0.12$				
$^{37}\text{Cl}$	0	1000	31	$0.20 \pm 0.06$	202	12 <sup>a</sup>	$0.46 \pm 0.19^a$	$0.60 \pm 0.22$
	0	500	24	$0.25 \pm 0.08$				
	0	210	11	$0.50 \pm 0.22$				
	1	1000	111	$0.74 \pm 0.10$				

<sup>a</sup>Excludes the 145- and 202-keV resonances of Mughaghab *et al.*

the Mughaghab value becomes  $10^4 S_0 = 0.46 \pm 0.19$ , which is consistent with our value for  $0 < E_n < 210$  keV. The recent RIPL-2 value [28] is also consistent with our value. For  $^{35}\text{Cl}$  our  $S_0$  value is just consistent with the RIPL-2 and Mughaghab values; however, our value is based on many more resonances over a wider energy range.

In the  $^{35}\text{Cl}$  case, our  $10^4 S_0$  is consistent with the spherical optical model (SOM) value of 0.6 [15]. In contrast, our  $^{37}\text{Cl}$   $10^4 S_0$  value for the energy range 0 to 500 keV is significantly lower than the SOM value of 0.7. This discrepancy could be due to misidentified  $p$ -wave resonances between 200 and 500 keV, since we find  $10^4 S_0 = 0.50$  for  $0 < E_n < 210$  keV.

The slope of the observed  $^{37}\text{Cl}$   $s$ -wave strength decreases significantly at about 200 keV; thus, there may be some misassigned resonances. We have assigned only seven  $^{37}\text{Cl}$   $s$ -wave resonances between 0.5 and 1.0 MeV. Experimental resolution coupled with the 24.2% abundance of  $^{37}\text{Cl}$  in natural Cl samples make it difficult to detect narrow-to-medium width resonances in this energy range. However, many missed narrow resonances and/or several resonances of width  $\sim 1$  keV would be required to increase the  $s$ -wave strength appreciably. For example, an additional seven resonances, either unobserved  $s$ -wave or misassigned  $p$ -wave, having neutron widths  $\sim 1$  keV would only increase the value of  $10^4 S_0$  from 0.20 to 0.30. The  $^{38}\text{Cl}$  structure could play a role in reduction of the  $s$ -wave neutron strength; for example, only 4 of the 39 bound levels in  $^{38}\text{Cl}$  have positive parity.

#### IV. CONCLUSIONS

The Cl data used in this analysis include recent ORELA high-resolution capture and transmission measurements as well as several older data sets. Since the  $^{35}\text{Cl}(n,p)^{35}\text{S}$  reaction yields a significant contribution to the total cross section from thermal energies up to about 10 keV, the  $^{35}\text{Cl}(n,p)$  data [12,13] were fit to obtain proton width values for several resonances. The proton widths are significant fractions of the total widths for resonances at 398 and 4251 eV.

Definite  $J^\pi$  values were assigned to 23  $^{35}\text{Cl}$  resonances and 6  $^{37}\text{Cl}$  resonances; 15 of these are new assignments. New  $J$  assignments for 18 additional levels were also made. We have deduced parameters for many more resonances over

a much wider energy range than previous analyses. Our results include the first reported  $p$ -wave strength function values for Cl nuclides. Average neutron widths, radiation widths, and level spacings were also calculated.  $S$ -wave neutron width and level spacing distributions for  $^{35}\text{Cl}$  are consistent with the Porter-Thomas and Wigner predictions, respectively.

When uncertainties are considered, there is good agreement between our resonance parameter calculations and experiment for  $^{nat}\text{Cl}$  total cross sections up to  $E_n = 1200$  keV, for  $^{35}\text{Cl}(n,p)$  cross sections up to  $E_n = 100$  keV, and for  $^{nat}\text{Cl}$  capture cross sections up to 500 keV. Energies, widths, and uncertainties were determined for 388  $s$ - and  $p$ -wave resonances; 246 resonances were assigned to  $^{35}\text{Cl}$  and 142 to  $^{37}\text{Cl}$ . Our thermal elastic, capture,  $(n,p)$ , and total cross sections are in good agreement with the corresponding ENDF/B-VI quantities, which are based primarily on the compilation of Mughaghab [15]. The agreement with ENDF/B-VI continues up to approximately 10 eV. In contrast, our resonance parameter representation fits the data from 10 eV to 1.2 MeV much better than previous representations. Consequently, more reliable criticality safety calculations should ensue from use of these new parameters.

#### ACKNOWLEDGMENTS

It is a pleasure to acknowledge helpful discussions with Drs. P. E. Koehler, H. Derrien, J. A. Harvey, T. E. Valentine, G. Arbanas, and R. W. Roussin. We are indebted to Dr. C. Wagemans for sending us the  $^{35}\text{Cl}(n,p)$  data of Druyts *et al.* This research was sponsored by the U.S. DOE Nuclear Criticality Safety Program (NCSP) and the Office of Environmental Management under Contract DE-AC05-00OR227525 with UT-Battelle, LLC. One of us (T.R.) was partially supported by the Swiss NSF under Grant 2000-061031.02 and the PROFIL program 2024-067428.01.

#### APPENDIX: CHARGED-PARTICLE PENETRABILITIES

A routine has been implemented in SAMMY for computation of Coulomb penetrability  $P$ , shift  $S$ , and phase  $\phi$  as a function of incident neutron laboratory energy  $E_n$  for the reaction  $n + A_2 \rightarrow A_3 + A_4$ . A slightly modified version of the routine

COULFG of Barnett [29] is used to compute the Coulomb wave functions and their derivatives. Input quantities are  $E_n$ , charges, masses, the reaction  $Q$  value, and the channel radius  $a_c$ . Quantities computed are the wave number  $k$ ,  $\rho$ ,  $\eta$ , and  $P_L$ , where

$$\begin{aligned}\eta &= 4\pi^2 Z_3 Z_4 e^2 M / h^2 k, \\ k &= 2\pi [2M(E_{\text{c.m.}} - Q)]^{0.5} / h, \\ \rho &= ka_c, \\ M &= A_3 A_4 / (A_3 + A_4), \\ P_L &= \rho / (F_L^2 + G_L^2).\end{aligned}$$

$P_L$  is the penetrability for angular momentum  $L$ ;  $F_L$  and  $G_L$  are the regular and irregular Coulomb wave functions, respectively, as defined by Lane and Thomas [30], for example.

The shift  $S_L$  and phase  $\phi_L$  are computed from

$$\begin{aligned}S_L &= (\rho / \mathcal{A}_L) d\mathcal{A}_L / d\rho, \\ \cos \phi_L &= G_L / \mathcal{A}_L, \\ \mathcal{A}_L^2 &= F_L^2 + G_L^2.\end{aligned}$$

The code has been tested against the published  $F_0$ ,  $G_0$ ,  $F'_0$ , and  $G'_0$  values of Abramowitz [31] for the range  $0.5 < \eta < 10$ ;  $1 < \rho < 5$ . For  $\eta < 6.5$  ( $F_0 > 10^{-6}$ ), the region of practical interest for nuclear reactions, the agreement for  $F_0$ ,  $G_0$ , and  $P_0$  is better than one part in  $10^4$ . For  $0.5 \leq \eta \leq 6.5$ , the agreement for  $S_0$  is better than four parts in  $10^4$ . However, note that for  $\eta \leq 0.5$ ,  $|S_0| \leq 0.2$ . Calculated values for  $L = 1, 2, 3$ , and 4 are in good agreement with the tabulated values of Bloch *et al.* [32]. The correct asymptotic behavior is exhibited as  $\eta \rightarrow 0$ :  $P_0 \rightarrow \rho$ ,  $S_0 \rightarrow 0$ , and  $\phi \rightarrow \rho$ .

- 
- [1] K. H. Guber, R. O. Sayer, T. E. Valentine, L. C. Leal, R. R. Spencer, J. A. Harvey, P. E. Koehler, and T. Rauscher, *Phys. Rev. C* **65**, 058801 (2002).
- [2] N. M. Larson, Oak Ridge National Laboratory Report ORNL/TM-9179/R6, 2003 (unpublished).
- [3] R. O. Sayer, K. H. Guber, L. C. Leal, and N. M. Larson, in *Proceedings of the International Conference on Nuclear Data for Science and Technology*, Santa Fe, 2004, AIP Conference Proceedings, edited by R. C. Haight *et al.* (Melville, New York, 2005), p. 386.
- [4] P. G. Young, R. E. MacFarlane, and L. C. Liu, ENDF/B-VI MOD 1 Evaluation, February 2000, available at <http://www.nndc.bnl.gov>
- [5] W. M. Good, J. A. Harvey, and N. W. Hill, Oak Ridge National Laboratory Report ORNL-4937, 1973, p. 198 (unpublished); J. A. Harvey, private communication.
- [6] U. N. Singh, H. I. Liou, G. Hacken, M. Slagowitz, F. Rahn, J. Rainwater, W. Makofske, and J. Garg, *Phys. Rev. C* **10**, 2138 (1974).
- [7] R. M. Brugger, J. E. Evans, E. G. Joki, and R. S. Shankland, *Phys. Rev.* **104**, 1054 (1956).
- [8] S. Cierjacks, P. Forti, D. Kopsch, L. Kropp, J. Nebe, and H. Unseld, kernforschungszentrum karlsruhe Report KFK-1000, 1969 (unpublished).
- [9] R. M. Kiehn, C. Goodman, and K. F. Hansen, *Phys. Rev.* **91**, 66 (1953).
- [10] H. W. Newson, J. H. Gibbons, H. Marshak, R. M. Williamson, R. C. Mobley, J. R. Patterson, and P. F. Nichols, *Phys. Rev.* **105**, 198 (1957).
- [11] N. T. Kashukeev, Yu. P. Popov, and F. L. Shapiro, *J. Nucl. Energy A/B* **14**, 76 (1961).
- [12] P. E. Koehler, *Phys. Rev. C* **44**, 1675 (1991).
- [13] S. Druyts, C. Wagemans, and P. Geltenbort, *Nucl. Phys.* **A573**, 291 (1994).
- [14] R. O. Sayer, Oak Ridge National Laboratory Report ORNL/TM-2000/212, 2000, available at [www.ornl.gov/~webworks/cpr/rpt/108142\\_.pdf](http://www.ornl.gov/~webworks/cpr/rpt/108142_.pdf).
- [15] S. F. Mughabghab, M. Divadeenam, N. E. Holden, *Neutron Cross Sections*, Vol. 1, Part A (Academic, New York, 1981).
- [16] I. G. Schroder, M. McKeown, and G. Scharff-Goldhaber, *Phys. Rev.* **165**, 1184 (1968).
- [17] G. H. E. Sims and D. G. Juhnke, *J. Inorg. Nucl. Chem.* **31**, 3721 (1969).
- [18] Y. M. Gledenov, V. I. Salatski, P. V. Sedyshev, P. J. Szalanski, J. Andrzejewski, and A. Zak, in *Proceedings of the International Conference on Nuclear Data for Science and Technology*, Trieste, 1997, edited by G. Reffo *et al.* (Bologna, 1997), p. 511.
- [19] Y. M. Gledenov, L. B. Mitsina, M. Mitukov, Y. P. Popov, J. Rigol, V. I. Salatski, and F. Van Zuan, Joint Institute for Nuclear Research, Communication **P3-89-351**, Dubna, USSR, 1989 (unpublished).
- [20] P. E. Koehler, R. R. Spencer, R. R. Winters, K. H. Guber, J. A. Harvey, N. W. Hill, and M. S. Smith, *Phys. Rev. C* **54**, 1463 (1996).
- [21] H. Krauss, K. Grün, T. Rauscher, and H. Oberhammer, 1992, TU Wien (Vienna, Austria), code TEDCA (unpublished).
- [22] T. Rauscher, R. Bieber, H. Oberhammer, K.-L. Kratz, J. Dobaczewski, P. Möller, and M. M. Sharma, *Phys. Rev. C* **57**, 2031 (1998).
- [23] R. L. Macklin, *Phys. Rev. C* **29**, 1996 (1984).
- [24] C. E. Porter and R. G. Thomas, *Phys. Rev.* **104**, 483 (1956).
- [25] E. P. Wigner, in *Proceedings of the Canadian Mathematical Congress*. (Univ. of Toronto Press, Toronto, Canada, 1957), p. 174; *Ann. Math.* **67**, 325 (1958).
- [26] A. M. Lane, Oak Ridge National Laboratory Report ORNL-2309, 1957, p. 113 (unpublished).
- [27] R. F. Carlton, W. M. Good, J. A. Harvey, R. L. Macklin, and B. Castel, *Phys. Rev. C* **29**, 1980 (1984).
- [28] IAEA-CRP, Reference Input Parameter Library, Phase II (RIPL-2), IAEA-TECDOC, 2004, available at [www.nds.iaea.org/ripl2/](http://www.nds.iaea.org/ripl2/).
- [29] A. R. Barnett, *Comput. Phys. Commun.* **27**, 147 (1982); **21**, 297 (1981).
- [30] A. M. Lane and R. G. Thomas, *Rev. Mod. Phys.* **30**, 257 (1958).
- [31] *NBS Handbook of Mathematical Functions*, edited by M. Abramowitz and I. A. Stegun (U.S. GPO, Washington, DC, 1964), p. 537.
- [32] I. Bloch *et al.*, *Rev. Mod. Phys.* **23**, 147 (1951).